DEPARTMENT OF OCEAN ENGINEERING
MASSACHUSETTS INSTITUTE OF TECHNOLOGY
CAMBRIDGE, MASSACHUSETTS 02139

PENETRATION EFFECTS OF THE COMPOUND VORTEX IN GAS METAL-ARC WELDING

by

JOHN PATRICK SPENCER

Course XIII-A

May 1988

THESIS
S66778

T239248

PENETRATION EFFECTS OF THE COMPOUND VORTEX IN GAS METAL-ARC WELDING

by

JOHN PATRICK SPENCER

B.S., United States Naval Academy
(1980)

Submitted to the Department of
Ocean Engineering
In Partial Fulfillment of the
Requirements for the Degrees of

NAVAL ENGINEER

and

MASTER OF SCIENCE IN MATERIALS ENGINEERING

at the

MASSACHUSETTS INSTITUTE OF TECHNOLOGY

May 1988

© Massachusetts Institute of Technology 1988

The author hereby grants the U.S. Government and its agencies permission to reproduce and to distribute copies of this thesis document in whole or in part.

PENETRATION EFFECTS OF THE COMPOUND VORTEX IN GAS METAL-ARC WELDING

by

JOHN PATRICK SPENCER

Submitted to the Department of Ocean Engineering on
6 May 1988 in partial fulfillment of the requirements
for the degrees of Naval Engineer and Master of
Science in Materials Engineering.

ABSTRACT

Twenty-one constant current welds were made at DCRP currents from 204 to 358 A. Three experiments were conducted where the current was in the form of a very slow sawtooth waveform from 200 A to 380 A over a period of 50 seconds. Two low frequency pulsed current welds were made using a 650 A peak current and a 250 A base current at 50 percent duty cycles; at 30 Hz and 10 Hz. All welds were made bead on mild steel plate using constant current GMAW equipment and argon + 2% oxygen shielding gas. After welding, the plates were cut, ground, polished and etched with 12% nital solution to show depth of penetration.

The constant current welds showed that unlike its behavior in GTAW, penetration increases gradually over the current range tested. Also, the growth of the "finger" constituted nearly all of the total penetration increase indicating convective flows of increasing magnitude. The ramped current experiments reinforced the observation that penetration increases gradually over the current range examined. The weld pool was also observed to fluctuate, slightly depress and finally depress significantly as the compound vortex started to form, formed completely and then grew stronger. The low frequency pulsed gas metal arc welds realized very little penetration because the wire feed motor was not fast enough and the torch had to be raised causing severe arc spreading.

Thesis Supervisor: Dr. Koichi Masubuchi
Title: Professor of Ocean Engineering and Materials Science

ACKNOWLEDGMENTS

The author wishes to thank Professors Koichi Masubuchi and Thomas Eagar for their instruction, help and support. Also, much gratitude is due Dr. Greg Kolodziejczak, who provided not only aid and insight but encouragement and humor.

Most importantly the author recognizes the assistance of three very special ladies without who's cooperation this thesis would still be a small stack of illegibly scrawled notes. The first is my best friend, who fortunately is my wife, Arlene. The other two are Miss Jennifer Spencer and Miss Jacqueline Spencer who are pleased to have their daddy back. It is finally "later."

TABLE OF CONTENTS

I. Introduction
  1. Gas Metal-Arc Welding in Shipbuilding.................7
  2. Automated Welding.................8
  3. Tack Welds.................10
  4. Compound Vortex.................14

II. The Process and Variables of Gas Metal-Arc Welding
  1. Background.................17
  2. Electrode Melting Rate.................19
  3. Metal Transfer.................25
  4. Welding Equipment.................35
  5. Prediction of the Fusion Zone.................38
  6. Penetration Mechanisms.................43
  7. Summary.................47

III. Previous Work
  1. Compound Vortex in GTAW.................48
  2. Pulsed GMAW.................50
  3. Goal.................50

IV. Experimental Work
  1. Experimental Apparatus.................53
  2. Constant Current Experiments.................55
  3. Ramped Current Experiments.................56
  4. Low Frequency Pulsing Experiments.................59

V. Results and Discussion
  1. Initial Objectives.................61
  2. Discussion of Results.................64
  3. Observations During Ramped Current Experiments.................67
  4. Pulsing Strategy.................70

VI. Computer Model
  1. Conduction Solution.................72
  2. Comparison with Experimental Results.................75

VII. Conclusions
  1. Compound Vortex in GMAW.................82
  2. Growth of the Finger Penetration.................82
  3. Distributed Source Conduction Solution.................83
  4. Increased Penetration.................83

Appendices:
  A. Temperature Field Program
    1. Program Listing.................85
    2. Program Explanation.................93
  B. Computer Program Output.................98

References.................100

LIST OF FIGURES

Figure Page

1. Diagram of a tack weld..11
2. Longitudinal cut through a tack weld showing defects..13
3. Diagram of the compound vortex........................16
4. Effect of an electrode extension and welding current on electrode melting rate....................21
5. Dependence of melting rate due to anode heating on the magnitude of welding current..................23
6. Effect of arc length upon the melting rate of a mild steel electrode................................26
7. Concentration of electromagnetic force at the region of minimum sectional area....................29
8. Effect of diameter of drop on velocity during transfer..30
9. Effect of current on the size and freqeuency drops transferred in an argon-shielded arc...........31
10. Increase in transition current from drop to axial-spray transfer caused by increasing the electrode diameter.....................................34
11. Changes in transition current from drop to axial-spray and rotary spray arcs caused by changes in the electrode extension and diameter......36
12. Plots of constant dimensionless temperature over the operating parameter (θ/n).......................41
13. Plot of surface depression versus current observed by Lim..49
14. Typical time plot of current used in pulsed GMAW.....51
15. The experimental apparatus.............................54
16. Plot of sawtooth waveform used in ramped current experiments....................................58
17. Plot of penetration versus current for the constant current experiments..........................62
18. Diagram of weld cross section showing (A) total penetration and (B) finger penetration...............63
19. Plot of finger penetration versus current for the constant current experiments....................65
20. Plot comparing finger penetration to total penetration......................................66
21. Plot comparing penetration resulting from ramped current experiments to penetration resulting from constant current experiments..........................68
22. Plot of longitudinal temperature distribution for weld 1-1 predicted by the computer model.............77
23. Plot of transverse temperature distribution for weld 1-1 predicted by the computer model.............78
24. Plot of longitudinal temperature distribution for weld 1-2 predicted by the computer model.............79

25. Plot of transverse temperature distribution for weld 1-2 predicted by the computer model............80
26. Plot of predicted and experimental penetration values..................................81

LIST OF TABLES

Table Page

1. Values for C_R for various diameters of a mild steel electrode...................................24
2. Transition currents for DCRP arcs with steel and aluminum electrodes.................................33
3. Constant current experiments data....................57

I. INTRODUCTION

1. Gas Metal-arc Welding in Shipbuilding.

Welding is used in the shipbuilding industry almost exclusively as the joining process of choice. Certainly, many other industries use welding very extensively and the results presented here will have applications in those industries as well. But this study has been directed toward shipbuilding where a very large fraction of the overall construction cost of a ship is the cost of welding. This cost includes the welding tools and consumables, but by the very labor-intensive nature of the process, most of the cost is devoted to the employment of skilled welders. Welders can often represent forty to sixty percent of the workforce in a large commercial shipyard. The amount of gas metal-arc welding will vary from ship class to ship class and shipyard to shipyard depending on such things as the fixturing available, crane lift capacities and the details of the ship design. Electric Boat Division of General Dynamics at Quansit Point, Rhode Island, is able to make extensive use of submerged arc welding in the construction of submarines because of their "modular" ship design and extensive fixturing. But in the construction of most ships, it is safe to say that gas metal-arc welding is a very large fraction, if not an outright majority, of the welding in terms of man-hours and consumables expended.

The use of higher strength steels such as HY 100 and HSLA

100 require more complex welding procedures. These procedures include pre-heat, post-heat and total heat input restrictions. The end result of these complicated procedures is more time and effort expended by a more highly trained welder to join the two pieces of steel. Additionally, the welder must often have special qualifications and weld much more carefully. Then, the finished weld must be inspected and any defects or irregularities must be ground out and welded again. It is easy to see why such a process is time-consuming, labor-intensive and expensive.

2. Automated Welding.

It is a worthy goal to seek to automate the welding process, and in particular, the gas metal-arc welding process. Ideally, welding machines or robot welders could work tirelessly around the clock doing repetitive tasks with great accuracy and speed. The efforts of human welders could be applied to more complex and non-repetitive welding tasks. Ships could be built more quickly and at less expense.

The trouble with this "pipe dream" is that shipbuilding in this country is not well-suited to automation. Ships are built "from the keel up" and they are built "by system". A ship is built "by system" in that the hull is built first. Then the various systems are placed into the hull. The electrical distribution system, the fire fighting system, the internal communication system, the propulsion system, the ship control

system, the sanitary system, the compressed air system, the fuel system, the hydraulic system, the combat system and many more systems are placed in the hull. Obviously this is a simplification since many of these systems must be in place before the hull is completed but the concept is valid. This "build by system" concept often results in very little repetitive work that can be performed outside the hull. Most of the welding occurs in the forms of welding of plates to frames already in place and the welding of systems in location onboard. A "modular" concept is much better suited for automated welding and has many other benefits that are beyond the scope of this paper. In a modular design, the ship is divided into "zones". These zones are three-dimensional piecs of the ship that contain all of the system components passing through that zone. The zones are constructed as one piece remote from the ship assembly site, transported to that site and then assembled to form the ship. Cleverly designed zones will have a myriad of opportunities for repetitive welding that robot welders will be capable of performing. Modular ship construction is the standard operating procedure in Japan, Korea and many other places over seas and is beginning to gain popularity in this country.

Even with modular ship construction, there are problems with automated welding. Plates distort while welding them, fit-ups are not perfect, joints vary in width and depth, plate thicknesses vary and other, less predictable variations occur in the welding conditions. Automated welding systems for use in

shipbuilding need to be adaptable. Systems are already in use that can sense the changes in welding conditions and alter the welding parameters to accomodate these changes. These systems and systems like them, still under development, are capable of making changes in welding current, voltage, travel speed, torch height, arc length or almost any other welding parameter using a rule-based system to accomodate variations in the welding conditions. These systems can make the appropriate changes in the welding parameters, provided of course, that the appropriate changes are known. There are situations where human welders do not have easy solutions. Specifically, tack welds pose a problem that is not easily solved.

3. Tack Welds.

A tack weld is a relatively short weld used to hold the two pieces of metal in place during welding (figure 1). It is easy to see that once the fit-up of two large pieces of hull steel is performed, the shipfitters can not be expected to hold the pieces in place until a welder can join them. Tack welds are used to hold the workpieces in place while the welders work. Another use for tack welds has to do with the thermal distortion that occurs as a result of welding. Since the metal expands and tends to widen the joint as welding takes place, tack welds are used to prevent this distortion. For instance, on a long, straight weld; as the welder starts welding at one end, the other end of the joint spreads apart due to thermal expansion.

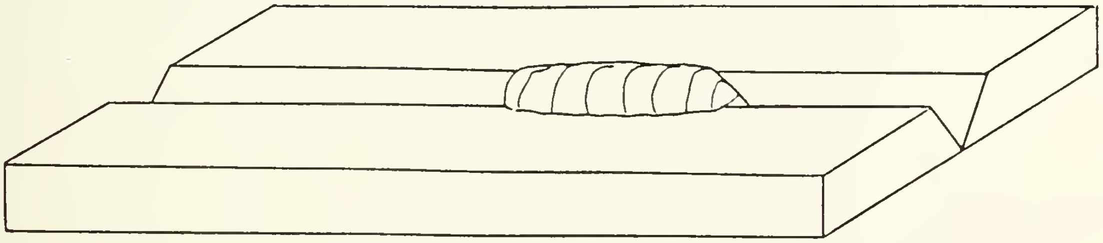

Figure 1. Diagram of a tack weld.

It may be impossible to weld these pieces until they cool if the gap becomes too wide. A tack weld, or series of tack welds, would prevent some of the distortion and allow the welding to take place.

Tack welds are usually performed by the shipfitters instead of welders. They are often performed hastily with the idea that a welder will soon cover this "temporary" weld with the finish weld that may involve several passes. They may even involve a different welding process, namely shielded metal arc (stick electrode) welding.

The problem caused by these tack welds is two-fold. Firstly, the presence of the tack weld causes a discontinuity in the welding process. The torch suddenly becomes closer to the weldment. And the normal flows in the weld pool are disrupted. Secondly, the tack weld, in effect, becomes a thicker section of metal to weld. To deal with this problem, the welder would require increased penetration and decreased metal deposition to avoid an unsightly mound or glob where he welded over the tack weld. This irregularity might cause the weld to fail the quality control inspection. It would then have to be ground out and welded again; an expensive and time-consuming process. Defects at the leading and trailing edges of the tack weld (figure 2), caused by disruption in the weld pool flow are common as well. These defects, discovered by non-destructive testing (NDT) methods, may also result in the weld being ground out and welded again.

The purpose of this effort then, is to examine a method of

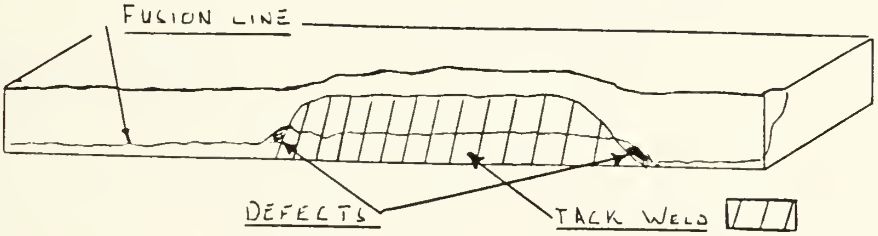

Figure 2. Longitudinal cut through a tack weld showing defects.

dealing with tack welds that could be employed by an automated welding system. This method employs a penetration mechanism know as the compound vortex. At the outset, it should be stated that although insight has been gained as a result of the author's work, the method envisioned as a means of dealing with tack welds, was largely unsuccessful.

4. Compound Vortex.

The next chapter of this paper deals with the fundamentals of gas metal-arc process and the variables involved. Since it is a chapter that may be skipped by the reader who is familiar with the process, a brief description of the compound vortex is warranted here.

If the weld pool was axisymmetric, magnetohydrodynamic theory predicts toroidal flow. That is, flow parallel and perpendicular to the axis of the arc. These flow patterns called "thermo-capillary" and "diffuso-capillary", are described in chapter two. The circumferential flow would be very small. Real weld pools are not axisymmetric, however, and the circumferential flow becomes significant above a certain threshold current. Lin and Eagar [1] demonstrated that observed weld pool depressions in gas tungsten-arc welds could not be explained by arc pressure alone. High speed photography of oxide particles on the surface of the weld pool showed angular velocities above twenty radians per second. The centrifugal effect of this motion causes a cavity in the center of the weld

pool. This allows the arc to impinge the weldment at a point below the surface. The result is a significant increase in penetration. The compound vortex is characterised by a region of constant angular velocity in the center (forced vortex), surrounded by a region of constant angular momentum (free vortex). A diagram of the compound vortex model is shown as figure 3.

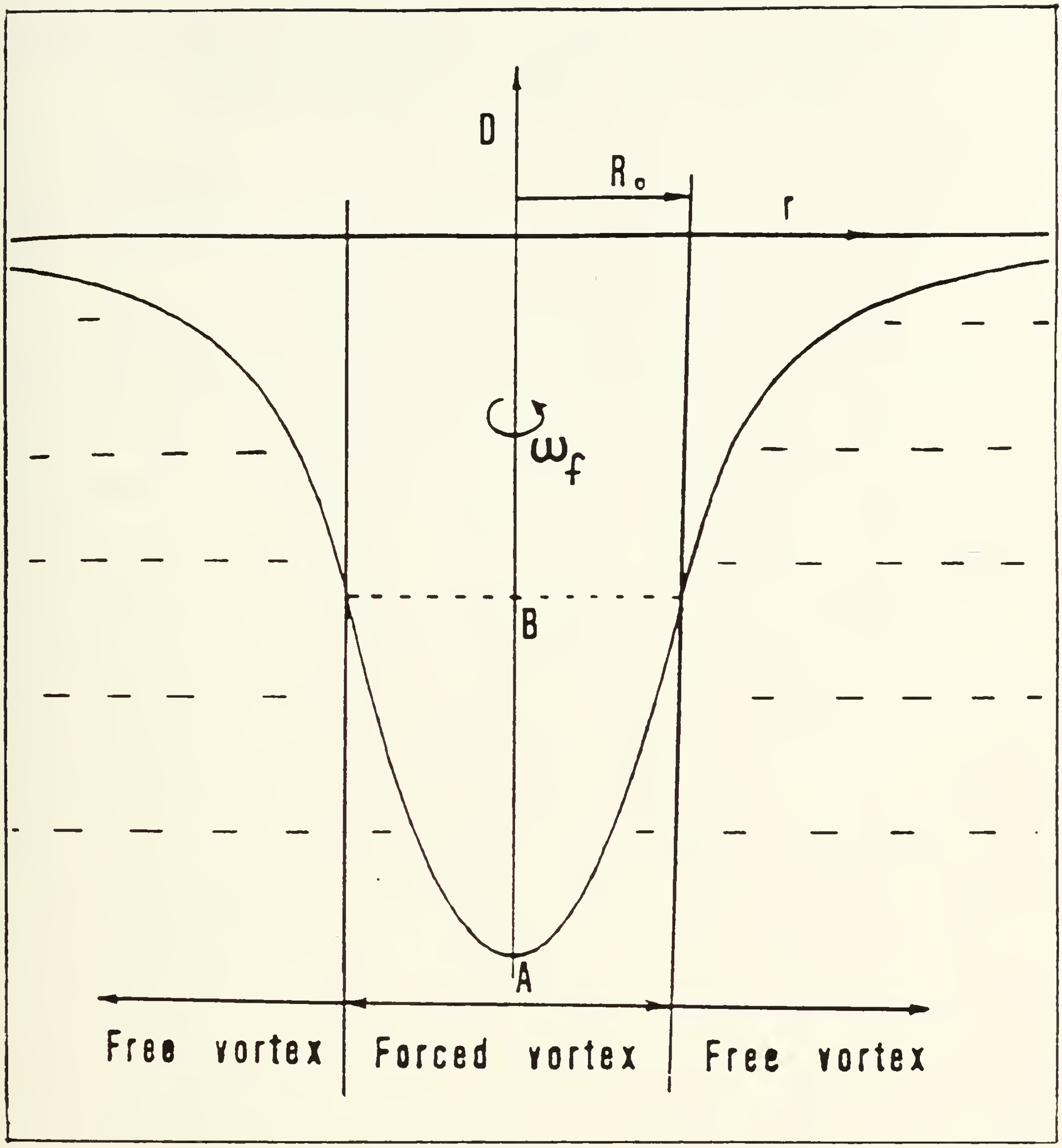

Figure 3. Diagram of the compound vortex [1].

II. THE PROCESS AND VARIABLES OF GAS METAL-ARC WELDING

1. Background.

In order to examine the process and variables of Gas Metal-Arc Welding, what is first required is a description of the process and an idea of how it differs from other joining processes. First of all, welding is a joining process used almost exclusively on metals, where the edges of the two workpieces are melted or fused together. Arc welding is the subset of welding processes that uses an electric arc to provide the heat needed to melt the metal. The first electric arc was struck over one hundred and seventy years ago by Sir Humphrey Davy in England. He described his experiment as follows: "When a current was sent by 1000 double plates, each 4 inches square, through potassium vapor between platinum electrodes, over a nitrogen gas, a vivid white flame arose. It was a most brilliant flame of from half an inch to one and quarter inches in length." [2] But it was not until eighty years later that Nicolas Benardos and Stanislas Olszewski patented a process that fused metal by striking an electric arc between a single carbon electrode and the metal workpiece. In 1892, Slavianoff proposed that a consumable electrode be used in place of the carbon electrode. Modified versions of this welding by stick electrode are still in use today.

Gas metal-arc welding is a welding process where the heat

required for fusion is provided by an electric arc struck between a consumable metal electrode and the workpiece. The electrode is a bare metal wire coiled on a spool that is fed at a measured (usually constant) rate to the torch where it makes electrical contact with the power supply. Thus the current flows from the contact in the torch, through the final inch or two of the electrode, to the arc. The molten metal in the arc and the molten weld puddle are protected from the atmosphere by a gas such as argon, helium or carbon dioxide which surrounds the arc and blankets the puddle. Otherwise oxygen and nitrogen from the atmosphere would readily combine with the molten metal and result in a weak, porous weld. [2]

Industry embraced arc welding as a marvelous innovation and began using it with very little understanding of how it worked. It was enough for industry to know that it did work. Much work has been done in this century to determine what variables affect the final weld and in what ways. Some of the important results of this work especially in the area of gas metal-arc welding will be summarized in this chapter. Before that can be done, some discussion of the process variables is required. This discussion will first cover electrode melting rate, metal transfer and welding equipment. Temperature distribution equations have been used to approximate the fusion zone and these will be discussed next. Finally, the current theories on weld pool motion and its effect on penetration and weld bead geometry will be explored.

2. Electrode Melting Rate.

There are two major sources of heat that contribute to the melting of the consumable electrode. [3] Firstly, heat is generated at the tip of the electrode. Most gas metal-arc welding is performed with the electrode positive (DCRP). In this case the electrode is the anode. Total heat transferred to the anode Q_A is

$$Q_A = Q_{CD} + Q_{CV} + Q_R + Q_E$$

where Q_{CD} is the heat transferred by conduction, Q_{CV} is the heat transferred by convection, Q_R is the heat transferred by radiation and Q_E is the heat transferred by electrons impacting the anode. Sanders and Pfender [5] found that heat transfer due to the electrons impacting the anode were responsible for up to 85 percent of the total heat transfer. They further described Q_E as follows:

$$Q_E = I\ (\ 5KT/2e + U + \phi\ )$$

where 5KT/2e is the electron thermal energy, U is the potential drop across the anode region of the arc, called the "anode fall" and ϕ is the potential energy surrendered by an electron upon entering a metal, called the electron "workfunction." The size of the boundary layer at the anode and the magnitude and shape of the anode fall in this region is the subject of some debate.

[5,9,10] The region under dispute is so small and temperatures so high that complete understanding of these phenomena is not currently available. But it is generally agreed that the bulk of the heat is carried by the electrons.

The second major source of heat occurs as a result of the electrical resistance heating caused by the current passing through the electrode.

Lesnewich [4] showed that heating due to radiation from the weld pool and the arc is negligible. Heat conducted by the molten tip of the electrode to the electrical contact point and then lost through conduction is also negligible under most welding conditions. [3]

Now that the two major sources of heat have been identified, it is left to examine the factors which affect them. Anode heating is affected by the current and electrode diameter but not the electrode extension. The melting rate due to electrical resistance heating is proportional to the electrode resistivity, extension and current squared but inversely proportional to its cross-sectional area. Electrode melting rates are generally independent of the shielding gas. [4]

Lesnewich studied gas-shielded metal-arc welding primarily using commercial mild-steel welding wire. [4] He determined that the contribution of anode heating to the electrode melting rate could be determined by measuring the melting rate at various electrode extensions and extrapolating the data back to an extension length of zero. Figure 4 shows a typical plot of the effect of electrode extension on electrode melting rate. At

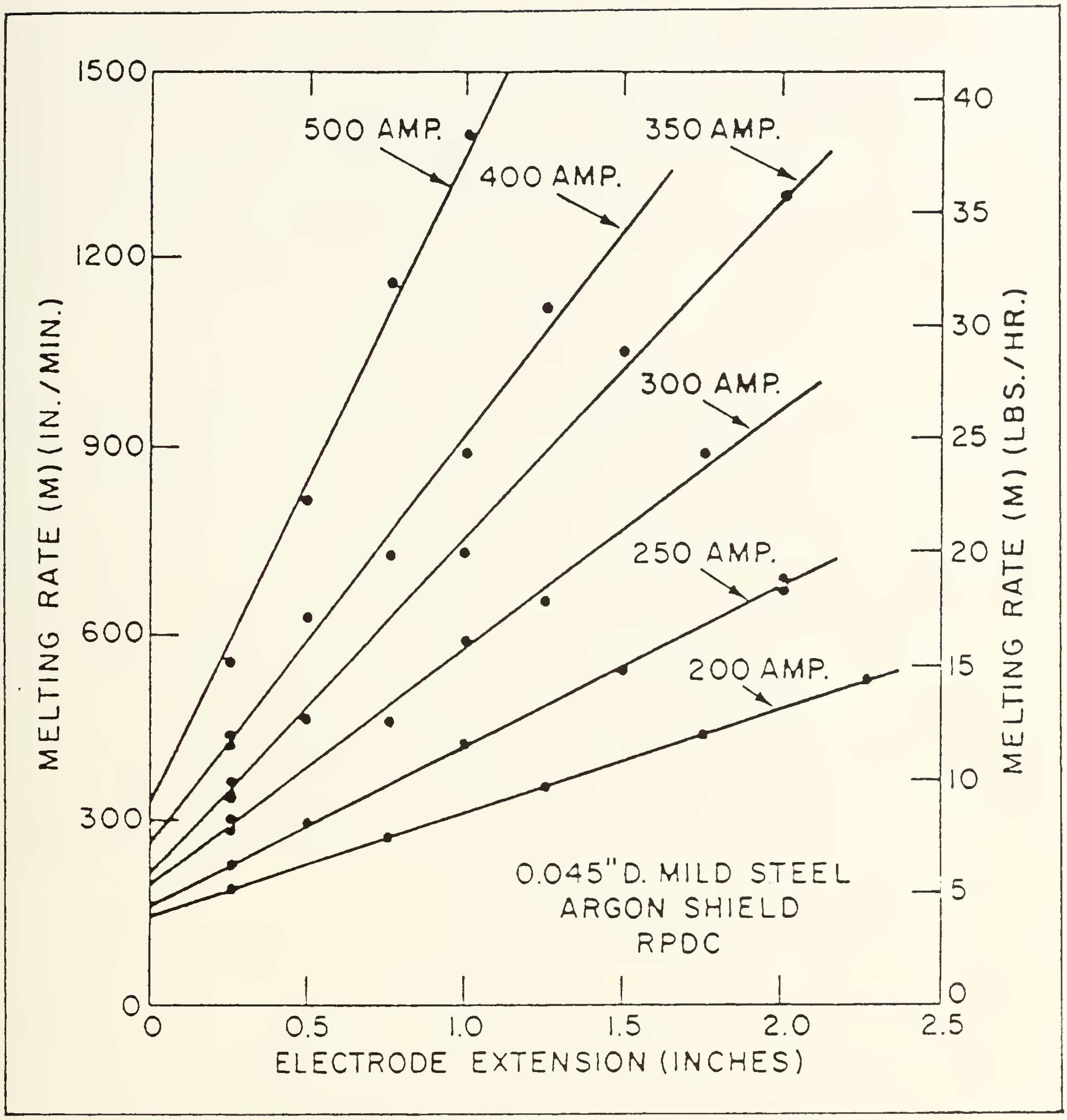

Figure 4. Effect of an electrode extension and welding current on electrode melting rate.[4]

zero extension, heating due to electrical resistance would be zero and the melting rate would be entirely due to anode heating. Lesnewich found that the melting rate due to anode heating, Ma, could be expressed as:

$$Ma = CaI$$

where Ca is the anode heating coefficient and I is the current. Ca is related to the anode drop and the electrode work function. It was shown that Ma is independent of arc length and electrode extension. The anode heating coefficient is dependent upon the specific heat of the electrode and its diameter. Figure 5 is a typical plot of anode melting rates as a function of current.

The voltage required to force current through a conductor is given by Ohm's law.

$$V_R = \rho \times L/A \times I$$

where: ρ = electrical resistivity

L = conductor length

A = cross-sectional area of the conductor, and

I = current flowing through the conductor.

Electrical resistivity is strongly dependent on the temperature of the conductor. This voltage drop, V_R times the current flowing through the welding electrode, I, is the heat energy due to the electrode's resistance, H_R.

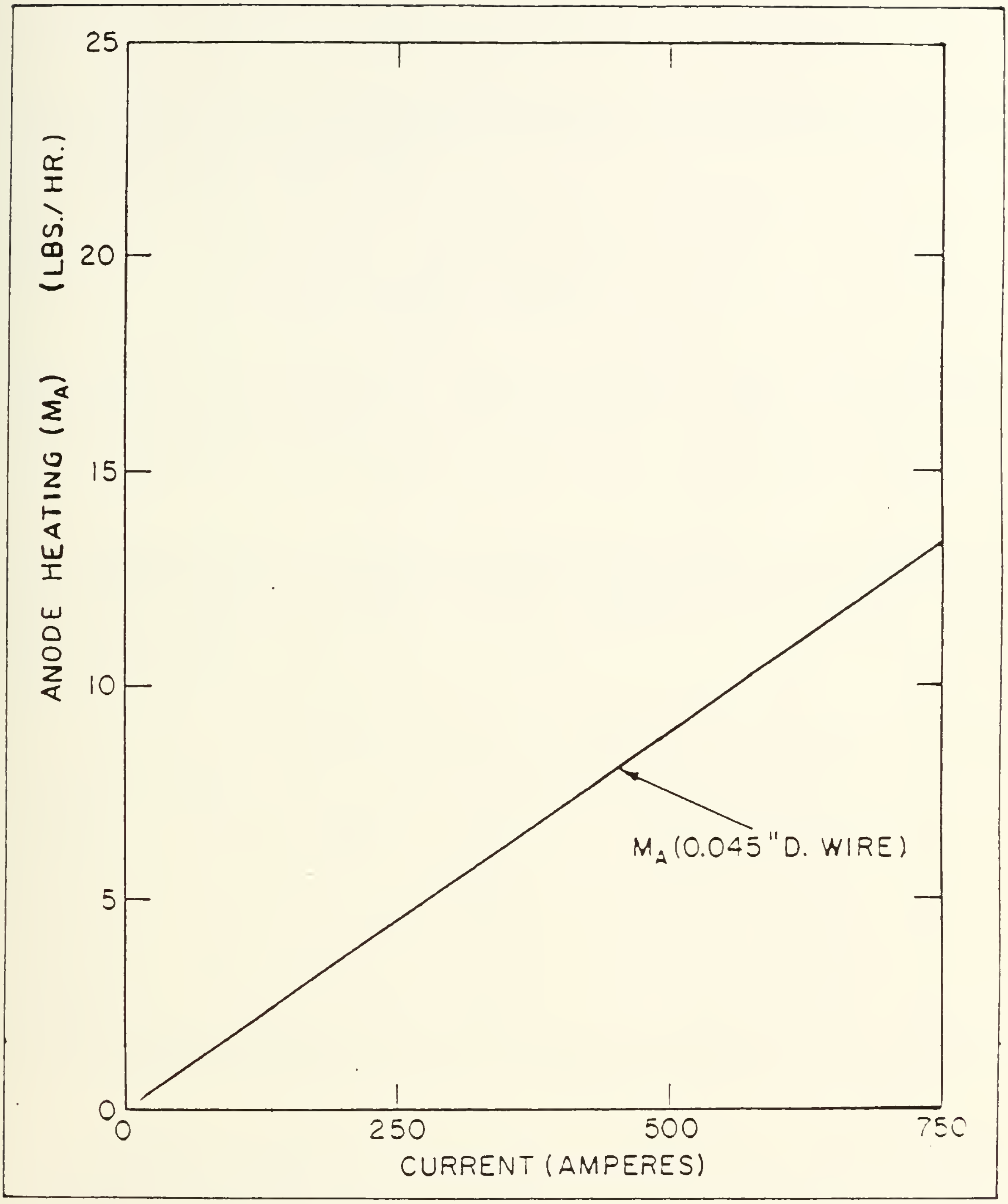

Figure 5. Dependence of melting rate due to anode heating on the magnitude of welding current.[4]

$$H_R = \rho \times L/A \times I^2$$

The equation for the melting rate due to resistance heating can be simplified to the form:

$$M_R = C_R L I^2$$

where C_R is a constant of proportionality that is dependent upon electrode diameter and the electrode resistivity. [4]

Table 1. Values for C_R for various diameters of a mild steel electrode [4].

	C_R	
Diameter (in)	in/(min amp^2 in)	lb/(hr amp^2 in)
0.030	260.0 x 10↑-4	313.0 x 10↑-6
0.045	42.1 x 10↑-4	114.0 x 10↑-6
0.062	10.5 x 10↑-4	54.7 x 10↑-6
0.093	1.6 x 10↑-4	19.2 x 10↑-6

Lesenwich found an exponential relationship between the cross-section area of the electrode and the resistance heating coefficient, C_R, as follows:

$$C_R = \frac{3.69 \times 10^{-8}}{A^{1.26}} \quad (\text{lb/hr in Amp}^2)$$

or

$$C_R = \frac{5.0 \times 10^{-8}}{D^{2.56}} \quad \text{(lb/hr in Amp}^2\text{)}$$

This equation and the equivalent expression for the anode heating coefficient were combined to provide an empirical equation for the electrode melting rate for direct-current reverse-polarity gas metal arc welding with a mild steel electrode.

$$M_{RP} = \left(0.017 + 0.37A\right) I + \frac{3.60 \times 10^{-8} L I^2}{A^{1.26}} \quad \text{(lb/hr)}$$

It is worthy of note that arc length has very little effect on melting rate as shown in Figure 6. [4]

3. Metal Transfer.

Metal from the consumable electrode is transferred to the weldment when the electrode is melted and drops of metal fall or are propelled through the arc to impact the weld pool. Or, in the case of short-circuit transfer, metal is transferred when the electrode extends and comes in contact with the weldment. The resulting short-circuit and associated rise in current through the electrode causes the tip of the electrode to melt off. This "short-circuit" or "dip" mode of transfer, although very useful in many applications, realizes little penetration and so will not be discussed in any depth in this chapter.

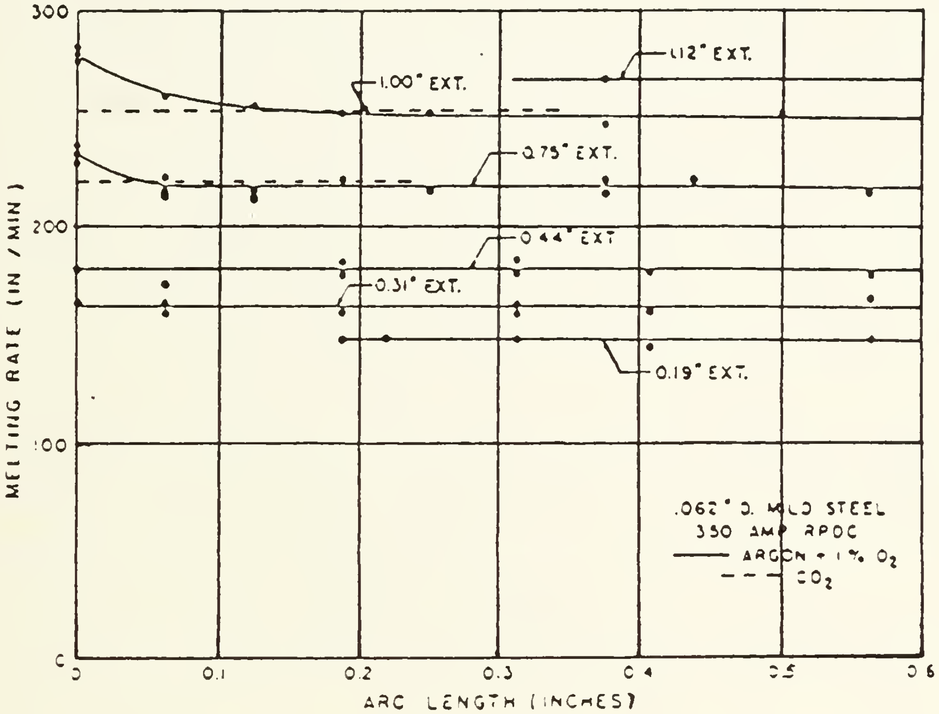

Figure 6. Effect of arc length upon the melting rate of a mild steel electrode.[4]

To cause the metal drops to travel across the arc, forces must act on the drops. The nature and magnitude of these forces have been the subject of some study. [3,6,7,8] A drop of molten metal is suspended from the tip of the electrode by surface tension. Surface tension is on the order of 1200 dynes/cm [3] for mild steel. In the case of a 1/16 inch (0.16cm) diameter electrode, this force would be about 600 dynes. This force must be overcome in order for the drop to travel across the arc. The force due to gravity is an obvious candidate. This force is equal to the volume of metal in the drop times the mass density of the molten metal (7.8 g/cm↑3 for steel) times the acceleration due to gravity (980 cm/s↑2). For a spherical drop of radius 0.1 cm this force equals 32 dynes. It would take a drop over half a centimeter in diameter to overcome the 600 dyne surface tension force. In fact, the force due to gravity could be considered negligible for drops smaller than the diameter of the electrode. Then there are other forces acting to propel the drops of molten metal from the electrode to the weld pool.

Two conductors carrying current in the same direction are known to attract each other. If the electrode is considered a bundle of current carriers there would be a force attempting to reduce the electrode's diamater. This force would not have a significant effect on a solid metal conductor but near the tip of the welding electrode, the conductor is in transition between its solid state and its molten state. This electromagnetic force tends to "pinch" off a drop and give an axial impulse. Reducing the diameter of the electrode has the added effect of

reducing the magnitude of the surface tension force. This force, often called the "pinch effect", acts independent of the polarity of the electrode. The total axial force is:

$$F = 1/2\ I^2$$

where I = the current in e.m.u. When the current is 300 ampere (30 e.m.u.) the force equals 450 dynes. Figure 7 shows that the electromagnetic force reduces the surface tension and concentrates the pinch effect. Consequently, a drop is pinched off along AA and is given an axial component of acceleration.

The drop then travels across the arc and impacts the weld pool at speeds that exceed gravitational acceleration alone. Masubuchi points out that a drop falling under the influence of gravity along a distance of 1/4 inch would achieve a speed of only 0.04 inch/s. [3] On the other hand, Jackson observed drop speeds of 15 to 50 ips as shown in figure 8. [9] This graph shows the drop speed decreasing as drop size increases. The knee of the curve occurs at a drop diameter of about 0.08 - 0.09 inches. It will be shown shortly that very small drops (diameter < 0.09 in) are transferred to the weld pool in the "spray" mode of transfer instead of the "globular" mode. Figure 9 shows that as welding current is increased, a rather dramatic change occurs at about 250 amprere. Lesnewich found that using reverse-polarity DC, with argon and 1% oxygen as the shielding gas, a "transition current" could be identified. At welding currents lower than the transition current, large drops of

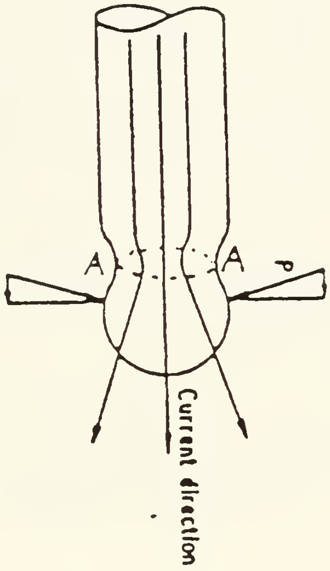

Figure 7. Concentration of electromagnetic force at the region of minimum sectional area.[3]

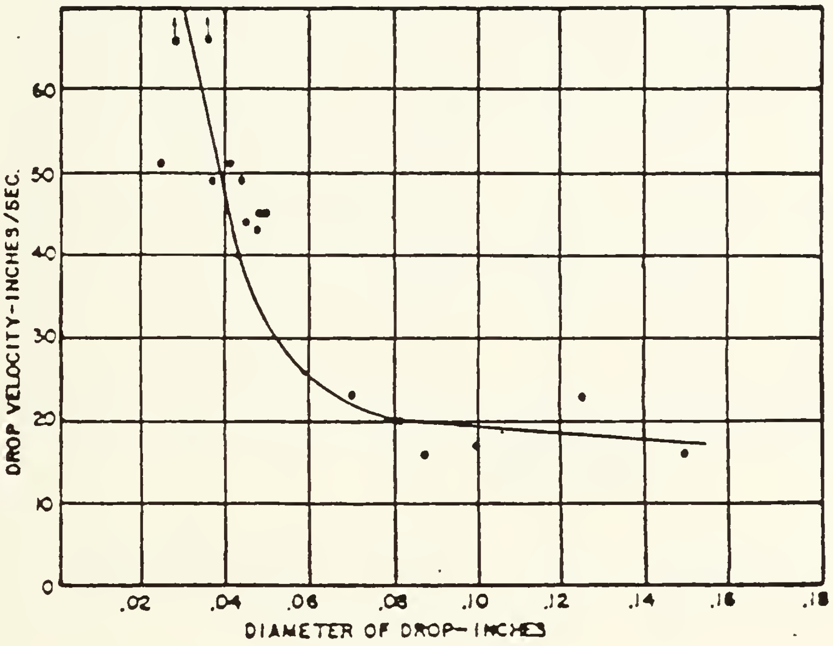

Figure 8. Effect of diameter of drop on velocity during transfer.[8]

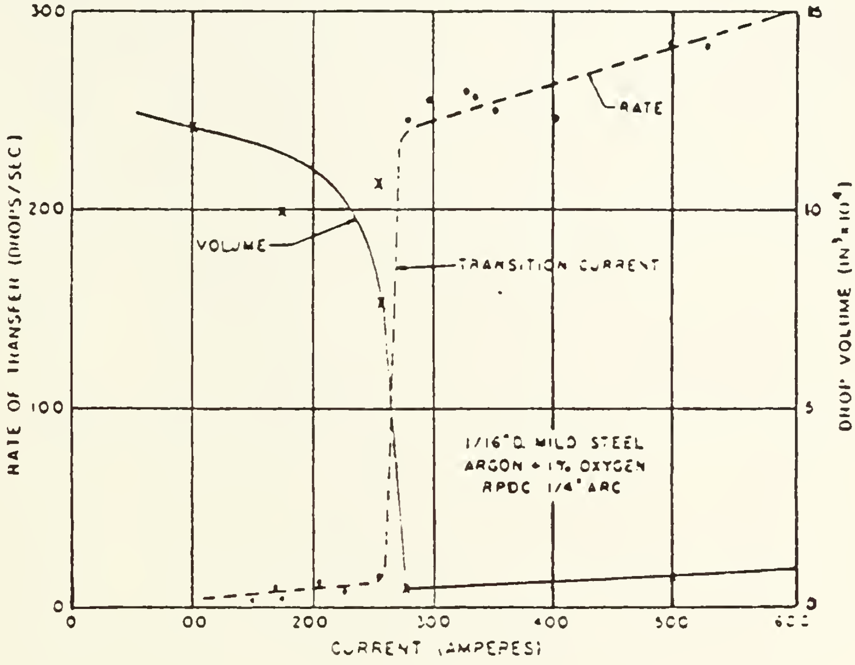

Figure 8. Effect of current on the size and freqeuency drops transferred in an argon-shielded arc.[7]

molten metal would be suspeneded from the end of the electrode until they "fell" toward the weld pool at a rate of only af few drops per second. Above this current, the metal was transferred in a "spray" of tiny drops at a rate of over 200 drops per second. Drops smaller than about 0.0005 cu.in. are transferred in the spray mode. This equates to a drop diameter of about 0.03 - 0.10 inches, or the knee of the drop velocity curve (fig. 8).

Spray transfer is desirable for greater penetration, increased arc stability and the fact that it allows overhead and out of position welding. The transition current is not a constant. It is dependent on many parameters including electrode composition, polarity, diameter and stickout length.

Table 2 lists the transition current for steel and aluminum electrodes of various diameters. Figure 10 shows the relationship between electrode diameter, stickout length and transition current for mild steel electrodes, under the welding conditions of DCRP and argon + 1% oxygen. The transition current for aluminum is less than that for steel and it decreases with smaller diameters and longer stickouts.

Lesnewich [7] proposed the following equation for transition current:

$$I = 60 + 3400\ D - 30\ L$$

where I = transition current in ampreres

D = electrode diameter in inches

L = electrode stickout in inches

TABLE 2.

TRANSITION CURRENTS FOR DCRP ARCS WITH STEEL AND ALUMINUM ELECTRODES [3]

Diameter mm	Transition Current (Amperes) Steel	 Aluminum
0.8	100	80
1.2	150	100
1.6	200	135
2.4	325	185
3.2	400	235

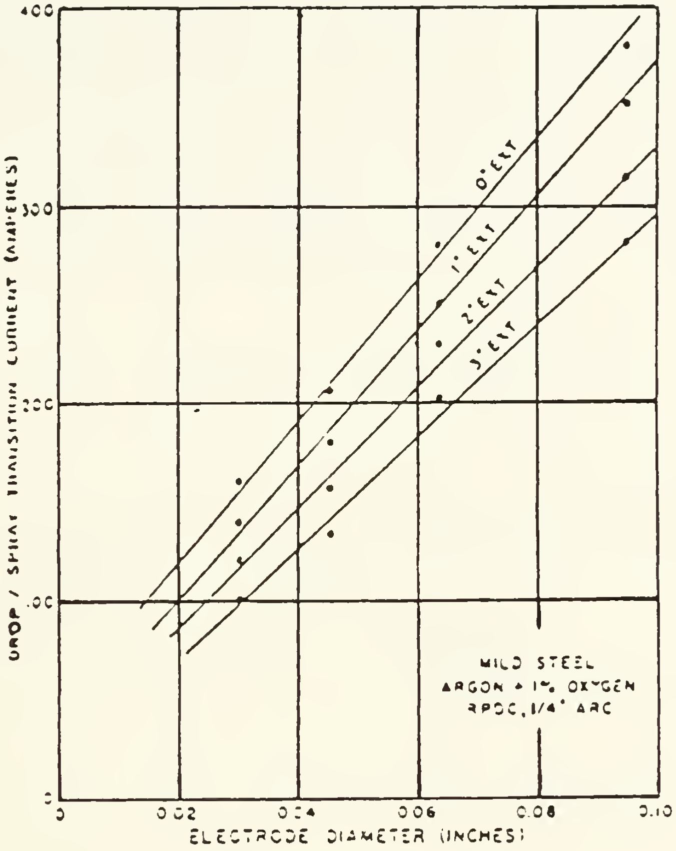

Figure 10. Increase in transition current from drop to axial-spray transfer caused by increasing the electrode diameter. [7]

Another transition occurs at even higher currents. Lesnewich found that above a certain threshold current, the tip of the electrode is bent and rotates around the axis of the electrode. This mode of metal transfer is called "spiral" or "rotating" spray. It results in much spatter and is not usually desirable. Lesnewich [7] proposed the following formula for transition from axial spray to rotating spray:

$$I = 25 + 1350\ D + 14.5 \times \frac{D^2}{L} \times 10$$

where I = the lowest current at which rotating spray is produced, in amperes

D = electrode diameter in inches

L = electrode stickout in inches

Figure 11 shows the relationship between the two transition currents and electrode stickout for three electrode diameters.

4. Welding Equipment.

At this point, some disuccsion of automatic gas-metal arc welding equipment is needed. The shielding gas, the consumable electrode and the electrical power must be provided to the welding torch in a coordinated fashion. The shielding gas is usually provided by cylinders of compressed gas regulated to the desired pressure and flow rate. It is channeled by means of a gas line to the torch where it surrounds the arc and covers the

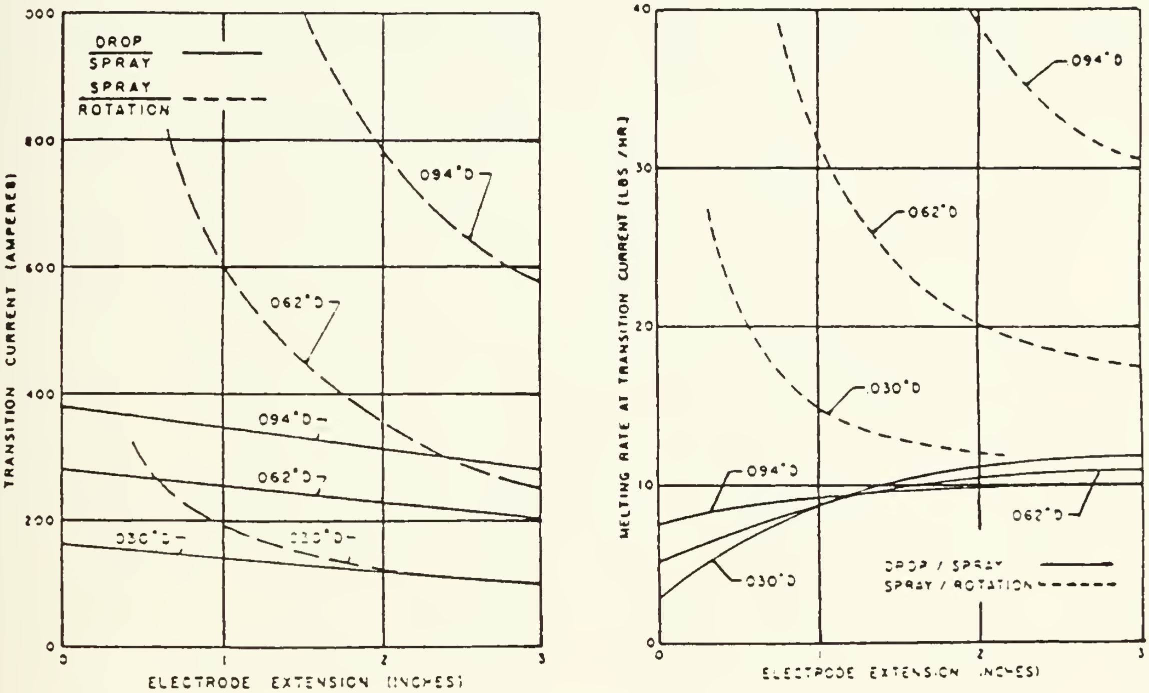

a. Transition Current

b. Melting Rate at Transition Current

Figure 11. Changes in transition current from drop to axial-spray and rotary spray arcs caused by changes in the electrode extension and diameter. [7]

molten weld pool. The consumable electrode is lead from a large spool across motorized rollers which push the wire through a conduit to the torch. The wire feed speed may be constant or variable depending on the control system. In its simplest form, the wire feed speed is set before welding and is maintained at a constant rate throughout the process. Some synergic control systems adjust wire feed speed as a means of compensating for variations in the joint to be welded. [12] At the torch, an electrical contact provides current to the electrode. A balance must exist between wire feed speed and electrode melting rate or the electrode would feed to quickly, piling up in the weld pool, or too slowly causing burn-back and damaging the torch. To provide this balance, a constant voltage source is used. The potential drops in the leads and torch are fairly constant and once the arc is established and the plasma is near some quasi-equilibrium, its potential drop depends only on arc length. So a constant voltage means a constant arch length for a given current. The power source adjusts the current to maintain a given arc length (i.e. arc voltage). If the arc gets too short, for a given torch height the stickout will be greater and this increases the electrical resistance heating which shortens the stickout and lengthens the arc. Simultaneously the shorter arc causes the power source to increase the current and this causes the melting rate to increase. If then the arc length becomes too long, these processes reverse to decrease the melting rate and increase the arc length so that a constant arc length is maintained. The most common set of welding conditions

for gas-metal arc welding of steel is DC reverse polarity (electrode positive) current with a shielding gas of argon plus small amounts of oxygen. [13]

In an experiment, welding a steel plate with a 0.045 in. steel electrode using DCRP and argon plus 2% oxygen as the shielding gas at a flow rate of 40 scf/hr, the welding voltage was set at 30 volts. The wire feed speed was set at 240 inches per minute because it was known that this would result in a current of around 220 amperes, a value very near the transition current. What resulted was a demonstration of the transition current and the manner by which the welding machine maintains a constant arc length. The metal transfer would be in the spray mode and the arc would become a little too long. The resulting reduction in welding current would cause the metal transfer mode to switch back to globular. The the arc would become too short and the increase in current would cause spray transfer again. The arc switched back and forth between globular and spray for the entire length of the weld.

5. Prediction of the Fusion Zone.

The weld metal is defined as that region of the weldment that has melted and resolidified during the welding operation. The fusion line is the boundary between the weld metal and the zone of metal, severly heated but not melted, called the heat affected zone. An isotherm of temperature equal to the melting temperature of the metal would exactly describe the fusion line.

Unfortunately, the heat transfer mechanisms at work in this tiny region are not completely understood and an accurate description of this isotherm has so far eluded investigators. Although Christensen [11] and Eagar [14] have made much progress in this area recently.

Christensen, Davies and Gjermundsen [11] generalized the temperature distribution equations deveoloped by Rosenthal and others. They developed the dimensionsless coordinates:

$$\lambda = \frac{V\ X}{2\ \alpha}$$

$$\psi = \frac{V\ Y}{2\ \alpha}$$

$$\zeta = \frac{V\ Z}{2\ \alpha}$$

$$\rho = \frac{V\ R}{2\ \alpha}$$

where V = travel speed

(x, y, z) = Cartesian coordinates moving with the heat source

$R = (x^2 + y^2 + z^2)^{1/2}$

α = average thermal diffusivity

Similarly, the temperature rise was rendered dimensionless.

$$\theta = \frac{T - T_o}{T_m - T_o}$$

where T_m = melting temperature of the metal is chosen as the reference temperature

Finally, they defined an operating parameter, n, such that

$$n = \frac{Q \quad V}{4\pi\alpha^2 c\gamma(T_m - T_o)}$$

where c = specific heat

γ = specific gravity

These terms were introduced into the Rosenthal equation for point heat sources moving across the surface of a semi-infinite body:

$$T - T_o = \frac{Q}{2\pi K}\,\frac{1}{R}\,e^{-\frac{V}{2\alpha}(R+X)}$$

where K = thermal conductivity = α(density)(specific heat)

The result was:

$$\frac{\theta}{n} = \frac{1}{\rho}\,e^{-(\rho+\lambda)}$$

Plots of constant θ/n in the range 0.001 to 100 are shown in figure 12. Large values of θ/n indicate a high intensity heat source and low weld speed. Small values of θ/n indicate a low intensity heat source and a high weld speed. The fusion line is located where θ = 1. The coordinates of the greatest width of any isotherm in terms of the radius vector are given by:

$$\lambda_m = \frac{-\rho_m^2}{1+\rho_m}$$

$$\psi_m = \zeta_m = \frac{\rho_m}{1+\rho_m}\sqrt{1+2\rho_m}$$

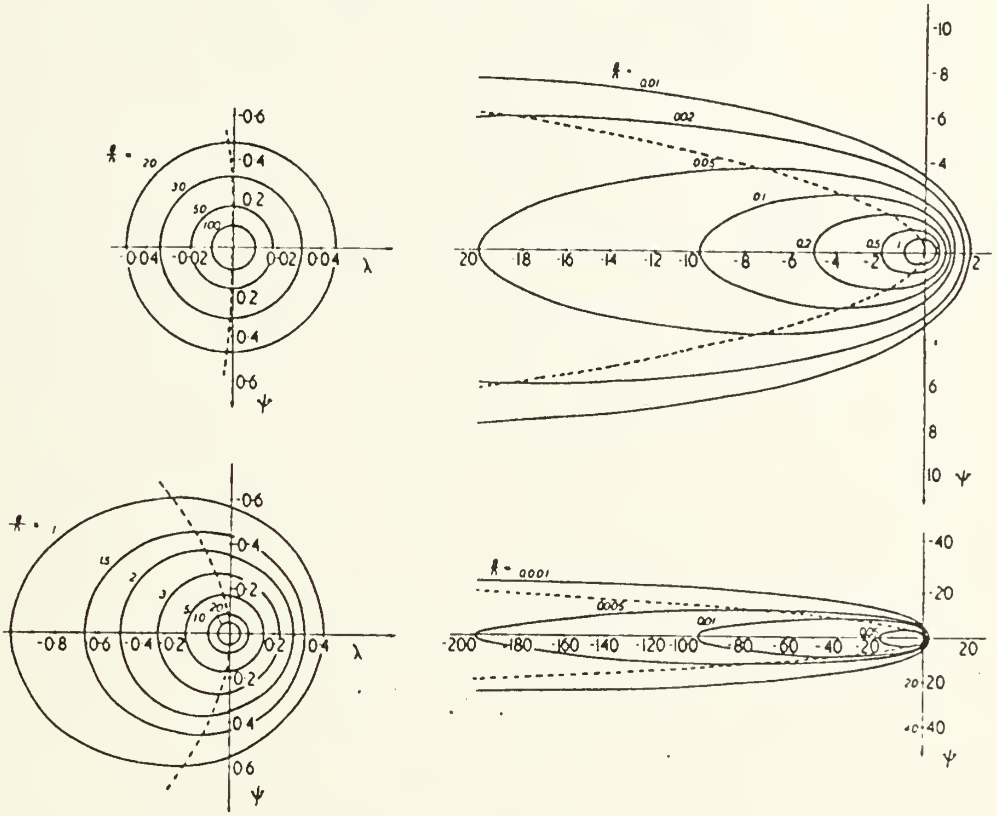

Figure 12. Plots of constant dimensionless temperature over the operating parameter (θ/n). [10]

A direct relationship is given between the operating parameter and ρ_m

$$n = \theta_m \rho_m \, e^{\left(\rho_m + \lambda_m\right)} = \rho_m \, e^{\left(\frac{\rho_m}{1+\rho_m}\right)}$$

The semi-circular contour predicted by these results was not borne out in Christensen's experiments. These temperature distributions were determined to be accurate at ranges far from the source but did not adequately predict the fusion line, the scatter amounting in some cases to a factor of two. Christensen did however have good results in predicting fusion zone cross-sectional area. Part of the problem in predicting fusion zone shape is that the fusion zone is not large compared to the heat source, the welding arc, as assumed in Christensen's theory. Eagar and Tsai [14] achieved better results modeling the heat source as a Gaussian curve instead of the point source assumed by Christensen. Eagar and Tsai had good results in predicting fusion zone area and width but experienced considerable error in predicting depth. This was partly because of the semi-infinite plate assumption. The rest of the error is a result of depression of the surface of the weld puddle by arc forces and convection in the weld pool. These mechanisms were not considered in the models proposed by Christensen and Eagar.

6. Penetration Mechanisms.

Heat flow models fail to adequately describe the shape of the fusion zone bcause they do not take into account convective flows in the weld puddle. The molten metal is depressed by arc pressure and metal droplets impinging the surface. Radial and circumferential flows are established in three dimensions. These flow patterns are responsible for the deep "finger" penetrations observed as well as other oddly shaped fusion zones.

Essers and Walter [15], using a specially-designed plasma-GMA welding torch and a water-filled calorimeter, were able to isolate and measure the heat transferred to the workpiece by each of the three major sources of heat. They found that, of the total heat transferred to the workpiece, 34% (±3%) was transferred by convection, radiation and conduction from the arc, 41% (±3%) was transferred by the passage of current through the workpice and 25% (±5%) was transferred by the drops of molten electrode. They also found that although heat from the electric arc accounts for about 75% of the heat transferred to the workpiece, it can have only a very limited influence on depth of penetration. High speed cinematogrphy showed that each metal drop depresses or indents the surface of the weld pool. If the drop frequency is higher than about 200 Hz, the indentation does not have an opportunity to refill before another drop strikes it. So the drops impact the same small crater and the heat carried by the drops is transferred

efficiently to the bottom of the weld pool [15]. To increase penetration, f x p (frequency x momentum), or total momentum per second, should be increased.

Other researchers such as Mills [16] and Ishizaki [17] have also found that weld pool effects are most important in determining fusion zone shape.. The flow patterns of the liquid metal in the weld pool determine the depth and shape of the fusion zone. If one were to take a bucket filled with water and direct a garden hose "jet" downward at the center of the bucket, one would observe the water to flow downward in the center, upward along the sides of the bucket and radially inward at the surface. If, on the other hand, a distributed "spray" was directed at the surface of the water in the bucket, the bottom would be undisturbed. Likewise, Mills found that a constricted heat source established a circulation that travelled downward at the center, radially outward along the bottom, upward at the sides and radially inward at the surface. This circulation pattern causes much deeper penetration than circulation that travels radially outward at the surface. The latter can be established by a more distributed heat source. Ishizaki found that longer GTA arcs, subject to more spreading, resulted in much more shallow, broader fusion zones. And shorter, more constricted arcs produced deeper and narrower fusion zones.

A more recent study conducted by Oreper, Eagar and Szekely [18] discussed three sources of convective flow. Bouyant convective flow is caused when the warmer, less dense metal in the center of the weld pool rises and the relatively cooler,

denser metal at the fusion line sinks to the bottom of the weld pool (diffuso-capillary flow). Electromagnetic convective flow is caused by the diverging current path in the weld puddle, establishing a magnetic field which interacts with the current and results in $\vec{J} \times \vec{B}$ (Lorentz) forces. These Lorentz forces cause convective flow downward in the center, upward at the fusion line and radially inward on the surface (thermo-capillary flow). And surface tension driven convection is a result of the shear forces established by the temperature gradients. If the surface tension increases with temperature, as in the case of pure iron, diffuso-capillary flow results. If some impurities exist in the iron and the surface tension decreases with temperature, thermo-capillary flow results. Thermo-capillary flow (downward in the center) results in deep penetration whereas diffuso-capillary flow results in wide, shallow welds. In the case of arc welding, bouyant forces are very small compared to electromagnetic and surface tension forces. When the electromagnetic and surface tension forces act in opposite directions double circulation loops can develop. Oreper's finite elements model showed these double circulation loops and computed the magnitude of their velocities.

Lin and Eagar [1] observed depressions of the weld pool surface over 4 mm deep and showed using calculus of variations and measured values of arc pressure that arc forces alone could not cause depressions of that magnitude. The model showed that arc pressures could depress the molten speel surface only about 1.3 mm. High speed photography of oxide particles on the

surface of weld pools showed circumferential vortex motions in the liquid. Angular velocities between 20 and 30 radians per second were observed and good correlation was obtained between theoretical depressions caused by such angular velocities and actual weld pool depressions. Lin's "compound vortex" model is shown schematically in figure 3.

7. Summary.

The important variables in gas metal-arc welding affect the process in the following ways [22]:

An increase in--	will cause--
welding current	1) an increase in melting rate, and 2) an increase in penetration and weld width.
arc voltage	1) an increase in arc length, 2) an increase in weld width, and 3) possibly a slight increase in penetration due to increased heat input. But spreading of the arc due to its increased length tends toward less penetration.
electrode extension	1) an increase in melting rate, and 2) possibly less penetration in the case where excessive melt-off causes the arc to impinge the weld pool instead of base metal.
electrode diameter	1) a decrease in melting rate, 2) a decrease in penetration due to decreased current density, 3) an increase in weld width, and 4) possibly problems with spatter and a "wandering arc".
welding speed	1) a decrease in penetration.

III. PREVIOUS WORK

1. Compound Vortex in GTAW.

Chihoski [25] found that in gas tungsten-arc welding, penetration in steel increased gradually as the welding current was increased for currents below 200A. Then, in the current range 200 to 300A, a large increase in penetration was observed. Above this, very little increase in penetration was observed from 300 to 450A and a gradual increase again for current above 450A. Lim [1] attributed this increase in penetration to the formation of a compound vortex and the resultant surface depression. Figure 13 shows the surface depression Lim found in his work on GTAW of steel. In the current range 270 to 300A, a compound vortex formed causing a marked increase in depression of the weld pool. Upon reducing the current, Lim found less current was required to maintain the vortex than to establish it. Kolodziejczak [26] argued that in the current region 300 to 450A, penetration remained constant because the weld pool had already been depressed by the vortex much more than arc pressure could, so the current is being conducted into the sides of the cavity and there is insufficient heat delivered to the bottom of the cavity to cause further melting. Above 450A, arc pressure begins to dominate as the primary source of weld pool depression. Since arc pressure increases with current, penetration also increases..

This narrow current region causing a large increase in

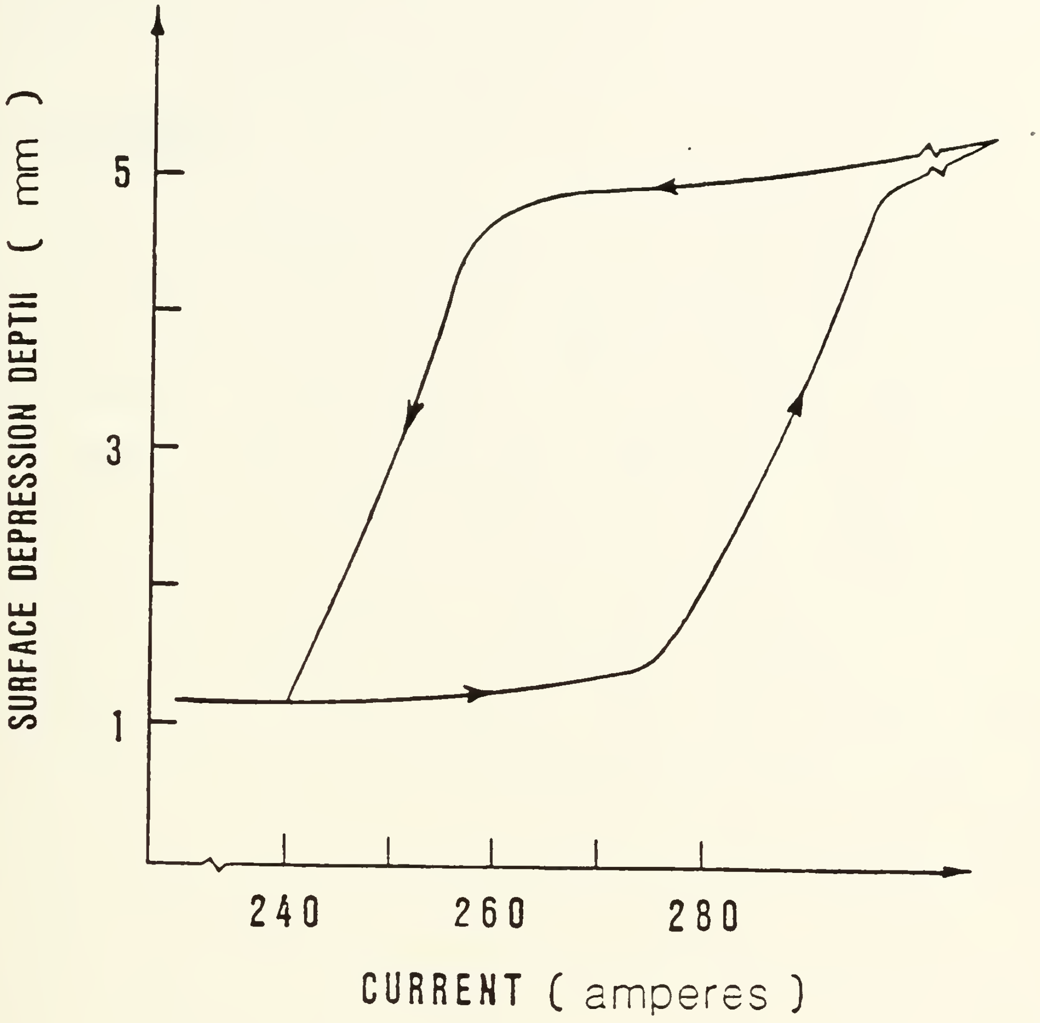

Figure 13. Plot of surface depression versus current observed by Lim. [1]

penetration provided hope that this phenomenon could be employed in some manner to yield high penetration welds with low average current.

2. Pulsed GMAW.

Kolodziejczak [26] studied pulsed gas metal-arc welding and the effects of various pulsing schemes on penetration and weld bead geometry. A representative plot of current versus time for pulsed GMAW is shown in figure 14. High peak current levels can be used in pulsed GMAW while maintaining lower average current by using a low base current. The lower average current results in lower heat input and less metal deposition. To take advantage of the compound vortex, the peak current must be higher than the threshold current and the duration of the peak must be longer than the time required to establish the vortex.

Most of Kolodziejczak's work was done at frequencies which were too high to allow adequate time for the formation of the vortex. Kolodziejczak sought to exploit other apparent resonances in weld pool motion to achieve larger penetration values.

3. Goal.

The goal of this work, then, was to determine:

a) if the formation of a compound vortex results in the same dramatic increase in

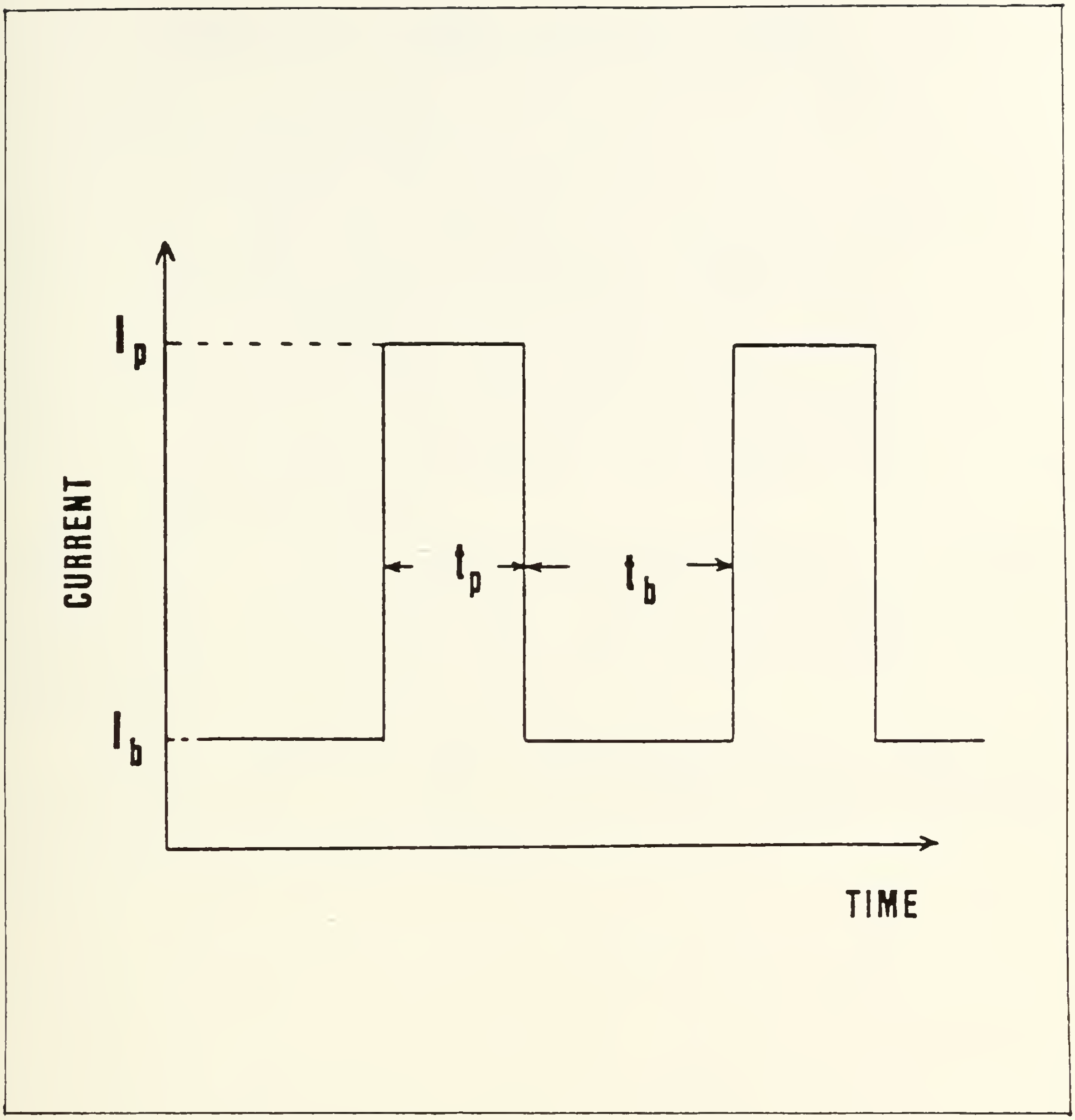

Figure 14. Typical time plot of current used in pulsed GMAW. [26]

penetration in GMAW as observed in GTAW,

b) the threshold current for establishment of a compound vortex in GMAW of steel,

c) the time required to establish the vortex at currents above the threshold, and

d) a methodology for employment of these findings to result in welds of increased penetration with little or no increase in average current.

The last point is consistant with the overall goal of a method to deal with tack welds that could be implemented by an automated welding system.

It was disappointing that this goal could not be met. It will be shown that a compound vortex affects GMAW penetration differtly than GTAW penetration.

IV. EXPERIMENTAL WORK

1. Experimental Apparatus.

All the welds were made by a stationary torch on moving plates. The plates were clamped to a water-cooled copper table moving at a constant travel speed perpendicular to the axis of the torch. (See figure 15.) Power was provided by two parallel Miller Gold Star 600SS power supplies through an Alexander Kusko 20KHz current regulator. A function generator sent a voltage signal to the current regulator which magnified the signal by 100 amperes per volt and provided the current to the welding torch. The voltage signal was also patched to an oscilloscope so that the signal could be viewed and adjusted before welding. All welds were performed with direct current, electrode positive (DCRP).

Mild steel wire (0.045 inch diameter) was provided from an overhead reel by means of a low inertia electric motor controlled by a logic circuit based on arc voltage feedback. Direct control of wire feed speed was not possible, so it was measured with a tachometer at the drive wheel. Cooling water was required for the current regulator, the moving copper plate and the torch. The shielding gas was argon with 2% oxygen provided at a pressure of 30 psig and a flow rate of 90 standard cubic feet per hour.

The arc length was maintained at 0.5 inch for all of the constant current welds. An optical system allowed viewing of

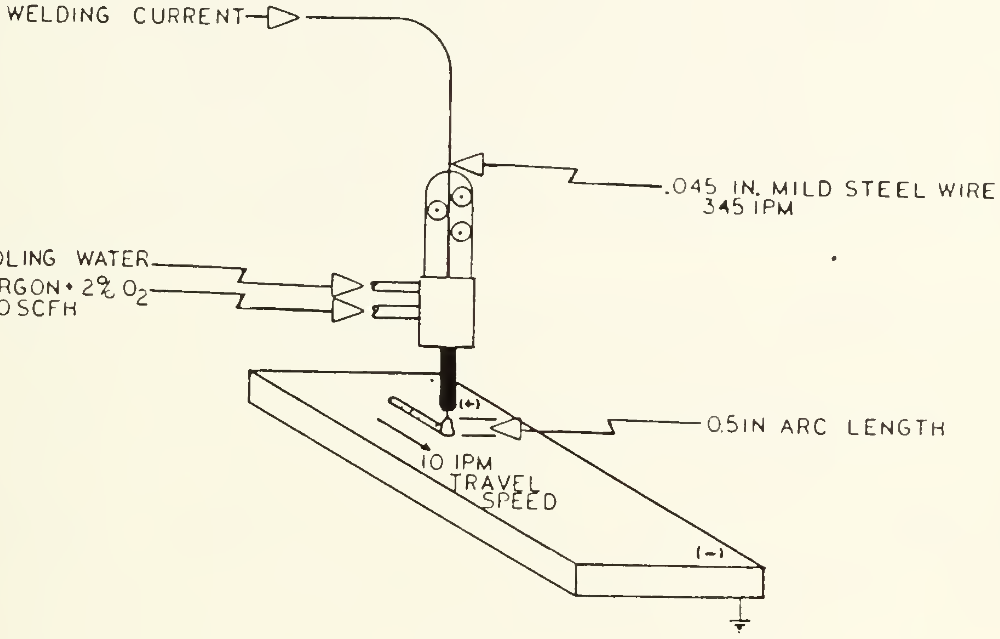

Figure 15. The experimental apparatus.

the arc while welding. Once the welding began, the torch height was adjusted to bring the arc length to 0.5 inch. The optical system consisted of a Melles Griot 5 mW He-Ne laser spread to a 20mm beam illuminating the arc and providing background light. A series of filters and lenses including a neutral density filter and a variable aperture, adjusted the ratio of background light to arc light. An RCA NewVicon color video camera then sent the resulting picture to a small video monitor in view of the operator.

Three sets of experiments were conducted on this equipment. The rationale behind each set of experiments will be discussed in chapter five. What follows here is a description of the experimental procedures. The three sets of experiments conducted were constant current experiments, "ramped" current experiments and low frequency pulsing experiments.

2. Constant Current Experiments.

A total of twenty-one welds were made, bead-on-plate, on 1018 cold rolled 12" x 4.5" x 3/8" mild steel plates at a travel speed of 10 inches per minute at various currents between 204 and 358A. Five or six welds were made on each plate after cooling the plate to ambient temperature between welds. The welds were each eight or nine inches long.

Three transverse cuts were made in the central region of the plates, away from the beginnings and ends of the welds. The three cross-sections were ground, polished and etched with a 12%

nital solution. Three separate penetration measurements were made for each weld and the results were averaged. Each measurement had an accuracy of about 0.25mm. Table 3 shows the current, voltage, torch height and overall penetration for each of the welds. During the second group of welds, the voltage meter was inoperative.

3. Ramped Current Experiments.

Three welds were performed with the current "ramped" from 200 to 380A. The signal generator was adjusted to provide a very slow sawtooth waveform such that only one full oscillation would be completed over the course of the weld. Since the travel speed was maintained at a constant 10 ipm, the welding current would be known at every point along the weld. The plot of current versus time (also current versus distance) is shown in figure 16. Maintaining the arc length at any given value was not possible for these welds. The increasing current and a more or less constant wire feed speed resulted in less stickout and, consequently, longer arcs at higher currents. These welds were made, bead-on-plate, on 1018 cold rolled 12" x 4.5" x 3/8" mild steel plates as before. These plates were cut longitudinally, however, to reveal the centerline of the weld at all points along the length of the weld. The plates were ground, polished and etched with a 12% nital solution. The results of these experiments will be discussed in chapter five.

Table 3.

CONSTANT CURRENT EXPERIMENTS

Weld No.	Current (Amps)	Voltage (Volts)	Torch Height (cm)	Penetration (mm)
1-1	251	31.9	1.4	3.1
1-2	275	34.4	2.1	3.4
1-3	301	36.0	2.0	3.6
1-4	321	35.6	1.9	4.4
1-5	295	34.6	1.7	4.1
1-6	268	35.1	2.6	3.4
1-7	329	36.2	1.6	4.2
1-8	311	35.4	1.8	4.0
1-9	285	35.5	2.2	4.1
1-10	261	32.4		3.4
1-11	243	31.4	1.4	3.1
2-1	300		1.7	4.1
2-2	224		1.5	2.5
2-3	328		1.4	4.4
2-4	348		1.3	4.7
2-5	279		1.7	3.7
2-6	217		1.7	2.6
2-7	358		1.2	4.1
2-8	341		1.3	4.3
2-9	236		1.7	2.8
2-10	204		2.1	2.4

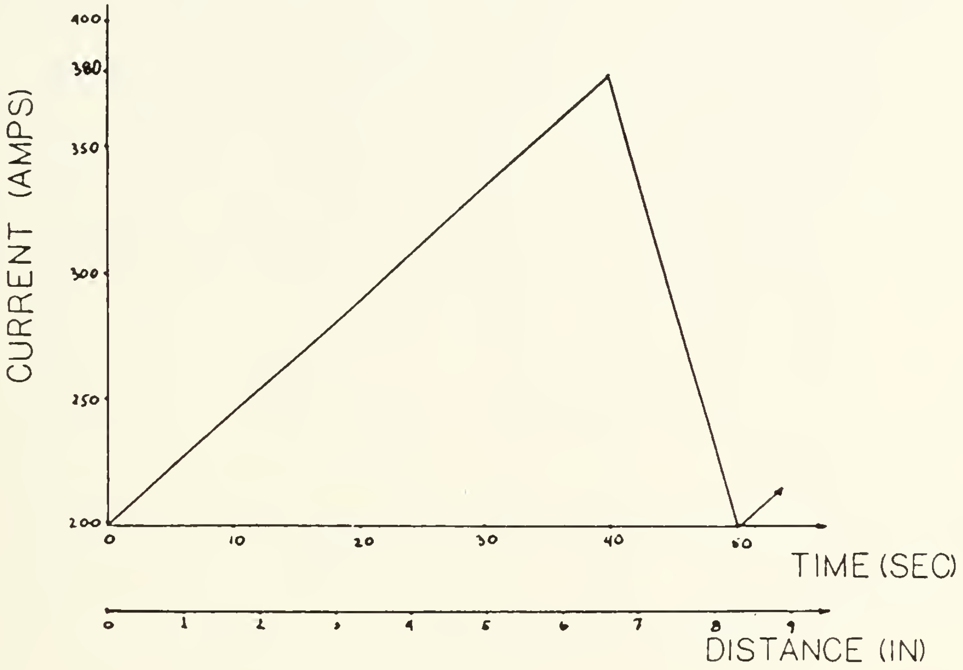

Figure 16. Plot of sawtooth waveform used in ramped current experiments.

4. Low Frequency Pulsing Experiments.

Two final welds were conducted using very low frequency pulsing. These welds were made, bead-on-plate, on 1018 cold rolled 12" x 4.5" x 3/8" mild steel plates just as before. The peak current was set at 650A and the base current was set at 200A with a 50 percent duty cycle. This resulted in an average current of 425A. Initially the torch height was adjusted to render a voltage of 36V and the travel speed was set at 17ipm so that the total heat input would be less than 55 KJ/in. Unfortunately, this resulted in burn-back and severely melted the copper contact tip inside the torch. Raising the torch allowed welding to proceed but the results were unsatisfactory.

The two welds were at 30Hz and 10Hz. Traces of the current versus time for these welds showed that the current dropped way off at the beginning of the pulse without ever reaching 650A and began to recover near the end of the peak pulse. Indications were that dynamic interactions between the inductance of the power supply and the capacitance of the current regulator may have been responsible for the problem. Kolodziejczak [26] experienced similar problems on the same equipment. Time was not available to isolate the problem and correct it in order to conduct the experiment over. The extreme torch height made this an infeasible method anyway, due to extreme spreading of the arc. A higher speed wire feed motor would have been required to lower the torch to a reasonable height without burn-back. A higher speed motor was available but it was incompatible with

the current regulator which was required to generate the square wave pulsed current. For these reasons the experiments were not conducted again.

As welded, the penetration was very minimal, averaging only 1.25mm. To avoid stubbing and burn-back with the torch at a reasonable height, a very responsive, high speed wire feed motor, with arc voltage feedback control would be required. The difficulty arises from having such a large variance between the peak and base current values and welding at such low frequencies.

V. RESULTS AND DISCUSSION

1. Initial Objectives.

The first two objectives stated at the end of chapter 3 were the determination of whether the compound vortex results in a substantial increase in penetration and what threshold current is required to establish a compound vortex in GMAW. In order to accomplish these objectives, twenty-one constant current welds were made. The resulting penetration was measured and plotted versus current in figure 17.

If the compound vortex behaved the same in gas metal-arc welding as in gas tungsten-arc welding, it was expected that a large increase, on the order of 1.25 mm [25], in penetration would occur around 250 to 290 A. Figure 17 shows no such sudden increase. What it does show is a gradual increase in penetration throughout the range of currents tested.

So at least the first objective had been obtained. Unfortunately, the result was that the compound vortex behaved differently in GMAW than in GTAW. Either the compound vortex did not form at all in this current range or the formation of the compound vortex did not result in a large increase in penetration. To gain some insight into this matter, another measurement was made on the weld bead cross-sections. Figure 18 shows a nominal weld cross-section. If A represents the overall penetration, then call B the "finger" penetration. The finger is that portion of the weld bead that extends down below the more or less semicircular region. The semicircular region might

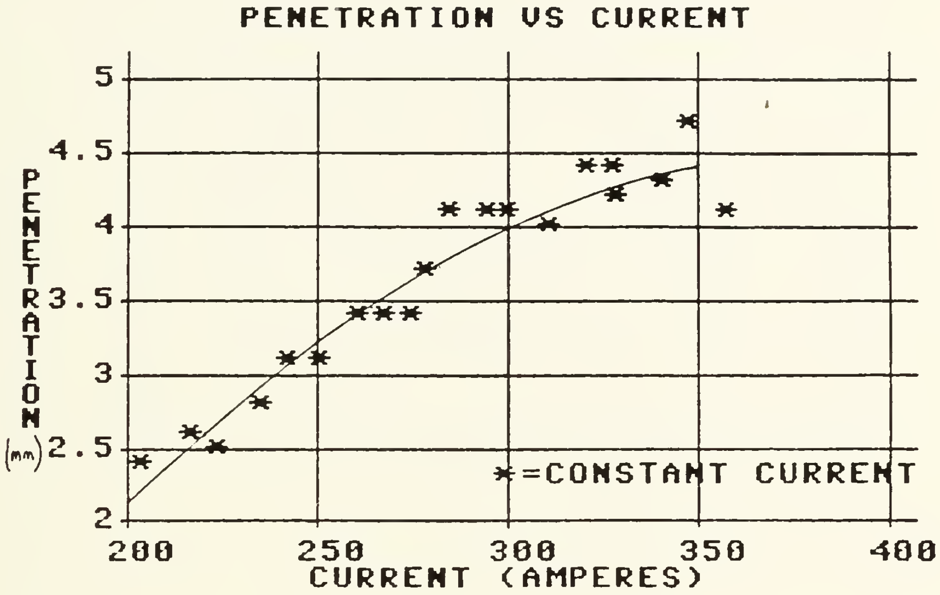

Figure 17. Plot of penetration versus current for the constant current experiments.

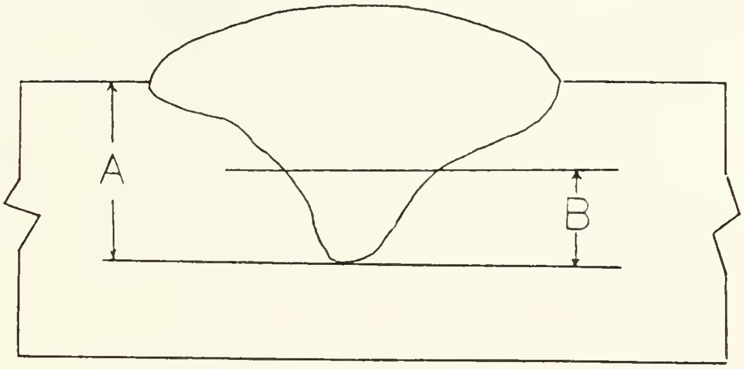

Figure 18. Diagram of weld cross section showing (A) total penetration and (B) finger penetration.

be thought of as that region of melting due to conduction heat transfer and the finger is due to convection and weld pool motion. It should not be misconstrued that these two heat transfer processes are independent and the total penetration could be obtained by summing the individual conduction and convection solutions (even if a convection solution existed, which at present it does not). If a (convection) heat transfer coefficient could be determined, by definition it would include both the conductive and convective mechanisms. The finger, however, would not exist if convection and weld pool motion did not occur. A sharp increase in finger penetration, in the current range of interest, would indicate the presence of the compound vortex. Figure 19 shows the results of the finger penetration measurements. Again, a steady increase is present instead of a large step that might indicate a threshold current.

2. Discussion of Results.

As current is increased, the penetration increases gradually over the entire range of currents tested. Further, the growth in the finger is also gradual over the entire range of currents. In fact, figure 20 shows that the growth in the finger accounts for nearly all the increase in penetration. The difference in the two curves in figure 20 results from growth in the conduction heat transfer due to the increase in heat input. But this growth is very small compared to the growth in finger penetration. So it is clear that weld pool motion in some form

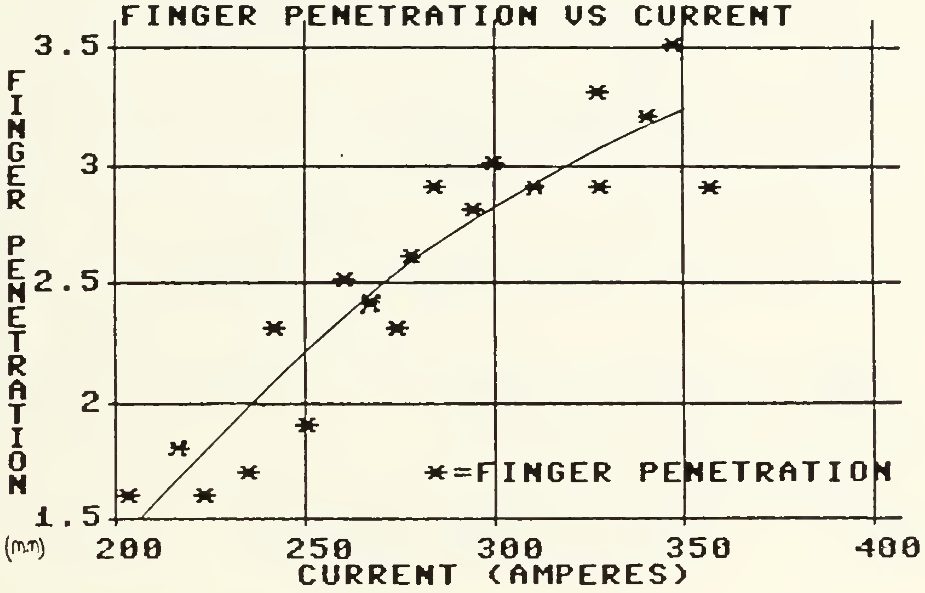

Figure 19. Plot of finger penetration versus current for the constant current experiments.

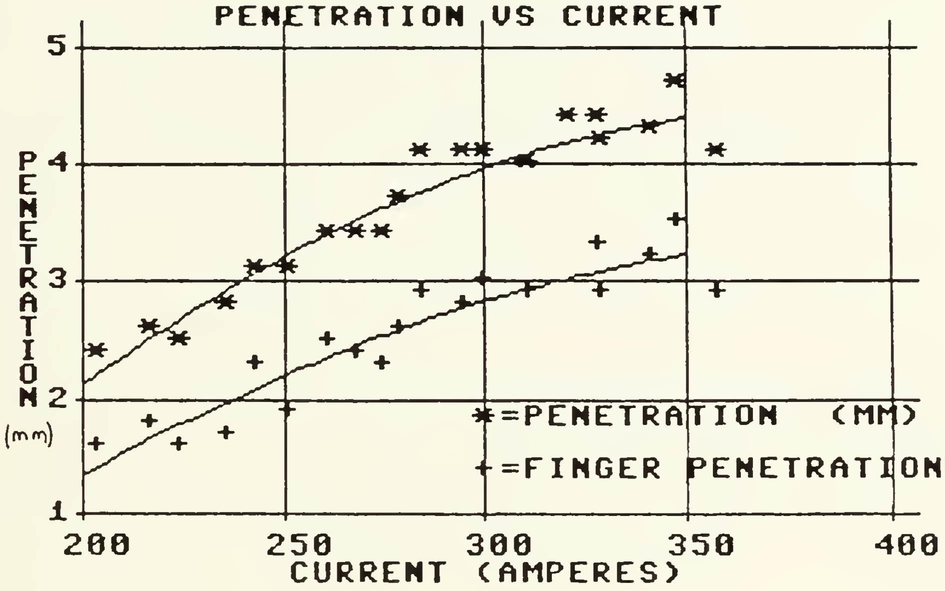

Figure 20. Plot comparing finger penetration to total penetration.

resulted in doubling the length of the finger while the depth of the semicircular region remained fairly constant.

The obvious candidate is the compound vortex. The gradual increase in penetration indicates that initially the vortex either partially forms or is disrupted by impacting metal droplets with no angular velocity. Then, as current is increased, the vortex is strengthened and enlarged as the weld pool grows in volume, so the impacting metal causes less disruption. The result is that instead of a sudden increase in penetration when the vortex is established as in GTAW, penetration, especially finger penetration, grows gradually as the vortex grows in strength and influence. To test this hypothesis another welding experiment was conducted.

3. Observations During Ramped Current Experiments.

The signal generator was adjusted to provide the slow sawtooth wave shown in figure 16. By allowing the current to increase in a continuous manner the weld pool depression could be observed. Also, by making a longitudinal cut to reveal the centerline of the weld, any sudden penetration increase would be clearly displayed. The results were plotted on the same graph as the constant current welds and are displayed in figure 21. The penetration values obtained from the ramped current experiment are represented by the almost linear curve (with no points) that falls between the overall penetration and the finger penetration. The fact that the arc length grew larger as

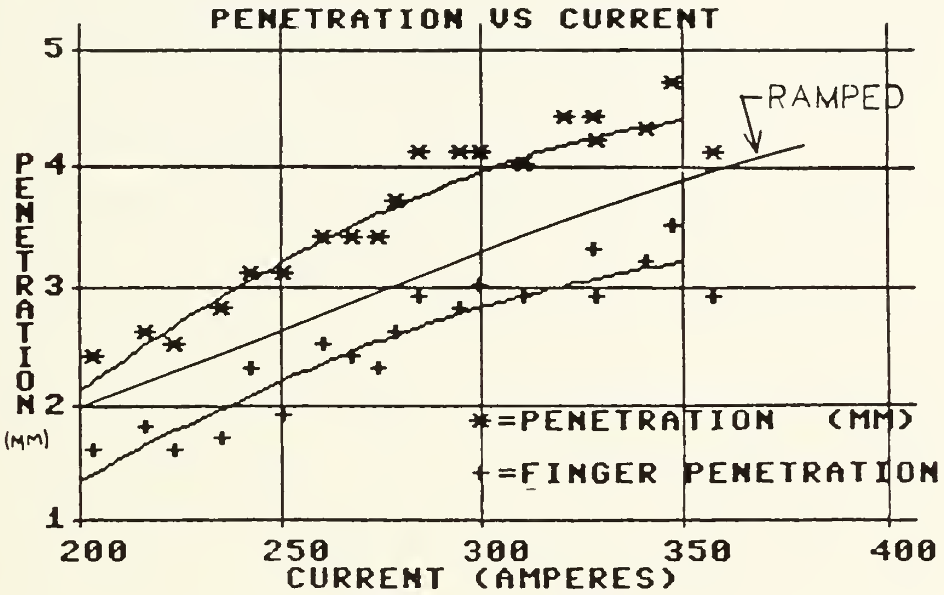

Figure 21. Plot comparing penetration resulting from ramped current experiments to penetration resulting from constant current experiments.

the current increased; allowing more spreading, explains why the ramped current experiment resulted in less penetration than the constant current experiments where the arc length was kept constant. It is interesting that since the arc spreading reduces the penetration due to conduction, the penetration obtained in this experiment grows at approximately the same rate as the finger penetration.

The other important observation during the ramped current experiments was related to the weld pool depression. As the welding current increased, the weld pool could be seen to fluctuate around 240 to 260 A, as if the vortex was alternately formed and extinguished. Then, at around 270 to 280 A, a distinct depression in the surface of the weld pool could be observed. At higher currents, the depression continued to grow in depth and become more distinct.

It appeared that the compound vortex began to form in the same general current range as in GTAW but that impacting metal drops with no angular velocity disrupted the formation. As the vortex strengthened with increasing current and the weld pool grew, the vortex formed and began to depress the weld pool surface. This resulted in an increase in penetration. But this increase in penetration did not occur over a short current range as in GTAW. A current increase of 100A (250 - 350A) resulted in about a 1.25mm increase in penetration. Another factor to consider was that this growth in penetration was due almost entirely to the growth in the finger. This may not be desireable in many welding geometries.

Refering again to the objectives stated in chapter 3, the first two had been obtained. It had been determined that the vortex behaved differently in GMAW than in GTAW but that it did result in an increase in penetration. The relationship between current and the formation of the vortex was also different in GMAW than in GTAW. No threshold current existed. The vortex began to form around 240 - 260A and was probably fully formed around 280 - 300A. It was clear that the third objective, that of determining the time required for the vortex to form, would now be very difficult to meet. Since there was no clear threshold current above which the vortex operated and below which the vortex did not. Also, the penetration measurements did not clearly show when the vortex was fully established and when it was not. So determining the time required for vortex formation was abandoned in favor of attempting to develop some method for employment of this mechanism.

4. Pulsing Strategy.

Recalling the problem of dealing with a tack weld by some automated system, it was desired that a sizeable increase in penetration could be realized with no increase in metal deposition and no increase in heat addition. Metal deposition and heat input are controlled by current. So it was attempted to invent a pulsing scheme that had a low average current and yet took advantage of the compound vortex for increased penetration. It was clear that to penetrate up to 10mm of tack

weld, a high peak current would have to be used and that the peak period would have to be substantial. To bring the average current down, a fairly low base current would have to be used and the base period would have to also be comparable to the peak period.

The experiment took the form of two welds using a square wave with peak current equal to 650A and base current equal to 200A. The peak period and base period were equal (50% duty cycle) resulting in a average current of 425A. A direct current weld of 425A was also conducted for comparison. Two frequencies were tested, 30Hz and 10Hz resulting in 16.7ms and 50ms peak periods respectively. It was attempted to adjust the voltage and travel speed so that the total heat input would be less than 55 KJ/in. (For many steels currently used in the construction of naval ships, heat input above this level requires special procedures and special qualifications for the welder.) Unfortunately this resulted in burn-back since the wire feed motor was not fast enough. Raising the torch resulted in unsatisfactory spreading of the arc and very poor penetration resulted. Additional problems encountered are discussed in chapter 4. Although success was not acheived in this experiment, low frequency pulsing warrants further study.

VI. COMPUTER MODEL

1. Conduction Solution.

Rosenthal's [27] equation for a moving point source of heat on a semi-infinite body is given in section 5 of chapter two. His assumptions were:

a) the thermal conductivity, specific heat and thermal diffusivity remain constant and are independent of temperature,

b) the heat input and the travel speed of the source are constant,

c) the source of heat is very small in size compared to the region of interest so as to be considered a point source of heat,

d) convective and radiative heat flows are neglected, and

e) the process has reached a quasi-steady state on a semi-infinite medium.

The last assumption provides that even though the temperature field is changing with time, the heat source is also moving and the temperature field is steady with respect the heat source. The coordinate parallel to the direction of motion (X), then can be converted into time by dividing by the travel speed. It is as if a thermal "snapshot" is taken of the workpiece as the arc passes by.

Eagar and Tsai [14] realized that the source of heat was not small if the the region of interest was the fusion zone. Their model used a distributed heat source approximated by a Gaussian function with standard deviation s.

$$T - T_0 = \frac{q}{Pi \times Ro \times C \times (4 \times Pi \times a)^{1/2}} \times$$

$$\int_0^t \frac{(t'')^{-1/2}}{2at'' + s^2} \exp\left[- \frac{w^2 + y^2 + 2wvt'' + y^2 t''^2}{4at'' + 2s^2} - \frac{z^2}{4at''} \right] dt''$$

where t'' = the integration variable

w = distance in the x direction in a moving coordinate system w = x - vt

v = travel speed of the arc

y = distance horizontally perpendicular to the direction of travel

z = distance measured vertically from the plate surface

q = net heat input per unit time (power)

Pi = 3.1415326536

Ro = mass density

C = specific heat

a = thermal diffusivity

s = arc distribution parameter

T = local temperature

To = initial temperature

This model was used in a computer program (Appendix A). The user inputed material constants, welding parameters, the type of "cut" desired (longitudinal or transverse) and where the cut was desired in relation to the arc. The program adjusted the values of w, y and z in 1mm increments and calculated the integral shown above by means of a twenty step Simpson's Rule process. Two virtual heat sources were added to approximate a finite plate instead of the semi-infinite plate assumed by Rosenthal.

The number of Simpson's Rule steps and the number of virtual sources was determined by trying several combinations and settling on a compromise of accuracy and program run time. The result obtained using twenty steps differs from the result obtained using 100 steps by less than three percent. The result obtained using two reflected sources differs from that using three sources by less than one percent. Some of the file commands and print statements in this program may be unfamiliar because the program was written to run on a Commodore 64C computer.

A sample of the output from this program is given in Appendix B. The data obtained from this program could be used to study the size of the fusion zone by examining the isotherm line equal in temperature to the melting temperature of the steel. The heat-affected zone could also be studied by locating the isotherm line of whatever temperature is determined to cause degradation in the properties of the steel. Cooling rates could be determined as well since the x coordinate functions as a time

variable. In this study, only the size of the fusion zone is of interest. The longitudinal cut was used to determine the maximum depth of the fusion zone. The transverse cut showed the basic shape of the fusion zone.

2. Comparison with Experimental Results.

The welding parameters for welds 1-1 and 1-2 were input into the computer program and the output data were plotted in figures 22 through 25. The melting temperature of mild steel is shown as a dashed line at 1539 degrees Celcius. Figures 22 and 24 show that the maximum depth of penetration occurs 0.6cm behind the arc. In weld 1-1 the maximum penetration is between the surface (z=0) temperature curve and the 3mm temperature curve. Interpolation of the data result in a penetration of 1.3mm. The maximum penetration for weld 1-2 is 4.4mm. The same procedure was carried out for other welding currents and the results were plotted in figure 26 along with the experimental results.

It is clear from figure 26 that the predicted results do not agree very well with the experimental results. A review of the assumptions made by Rosenthal reveals that even using a distributed source and a finite plate, there are two very important faults with the theory. The first is that the material properties of the plate do not remain constant as the temperature increases. And secondly, convective heat transfer is very important to the process. Additionally, not all of the

heat applied to the plate can be used to raise the temperature of the weldment. Since there is a change of phase (solid to liquid) some heat is lost as heat of fusion. These factors combine in a way that is not clear to change the slope of the current versus penetration curve. Another potential source of error is the calculation of the heat input to the plate. Appendix A and reference [6] show that the product of arc voltage and arc current is multiplied by an arc efficiency factor to determine the amount of heat applied to the plate. This arc efficiency is assumed to be constant when in fact it is a function of current. Reference [6] shows a plot (fig. 6.17 pg 164) of decreasing arc efficiency with total input power. An arc efficiency that is decreasing with current would help reduce the discrepancy between predicted and experimental results in figure 26.

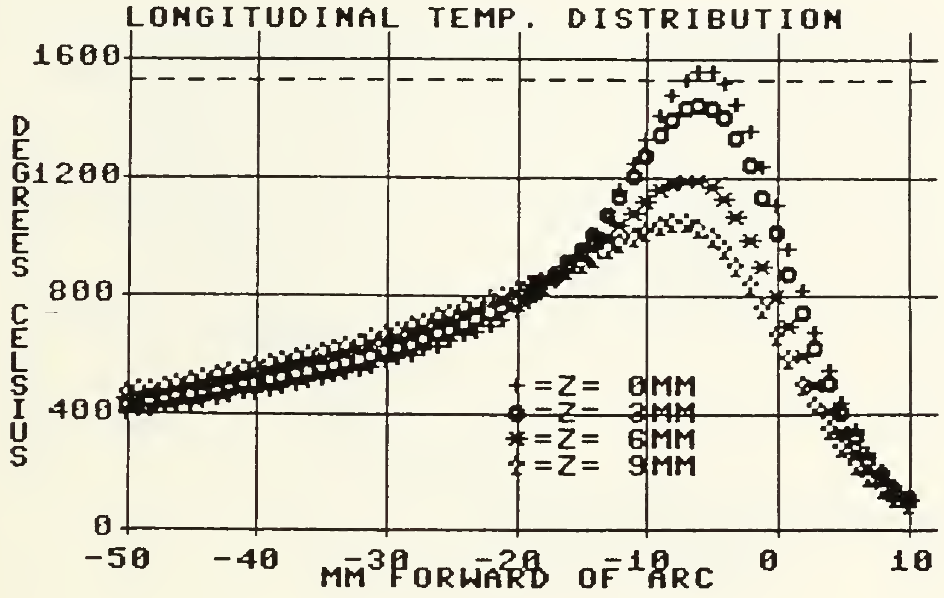

Figure 22. Plot of longitudinal temperature distribution for weld 1-1 predicted by the computer model.

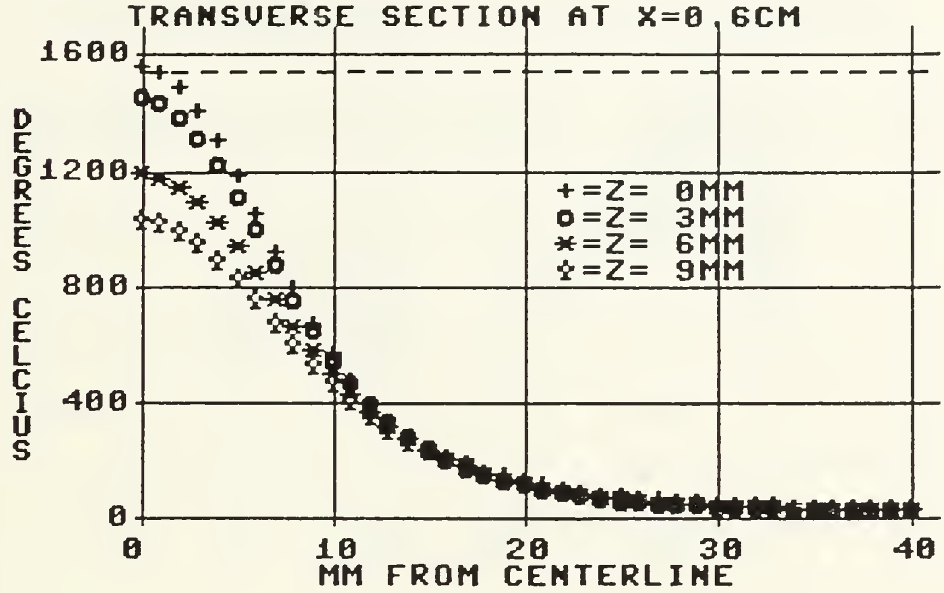

Figure 23. Plot of transverse temperature distribution for weld 1-1 predicted by the computer model.

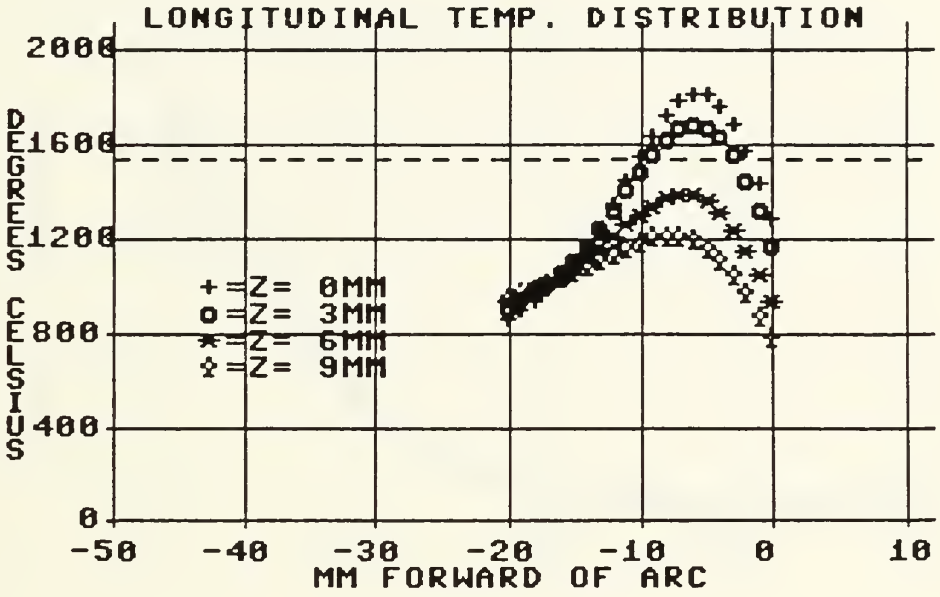

Figure 24. Plot of longitudinal temperature distribution for weld 1-2 predicted by the computer model.

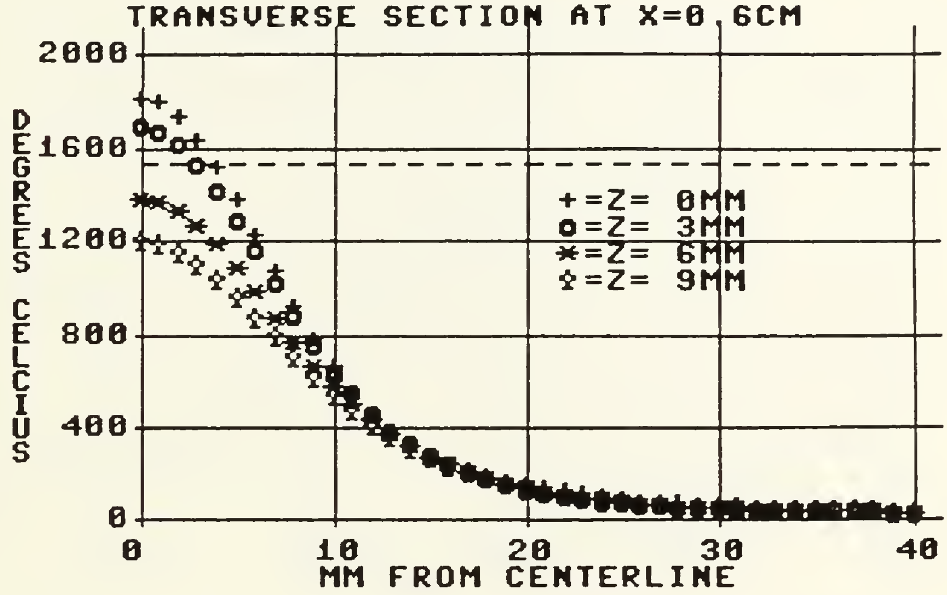

Figure 25. Plot of transverse temperature distribution for weld 1-2 predicted by the computer model.

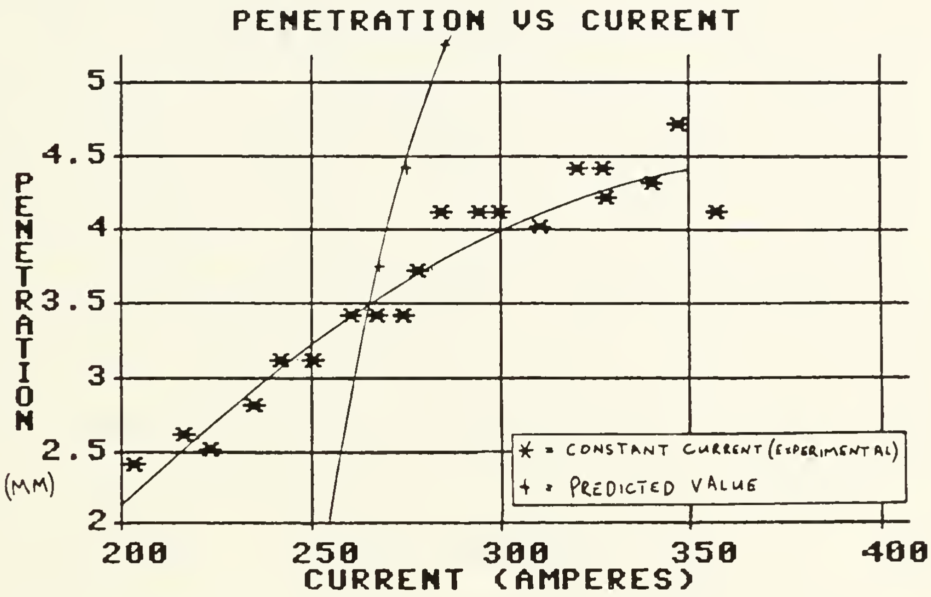

Figure 26. Plot of predicted and experimental penetration values.

VII. CONCLUSIONS

1. Compound Vortex in GMAW.

Unlike gas tungsten-arc welding where increased current brings about a sudden, very large increase in penetration when a compound vortex is established, increased current in gas metal-arc welding causes a gradual increase in penetration through the range where a vortex starts to form, forms completely and becomes very strong. Metal droplets from the electrode that impact the weld pool have no angular velocity and therefore have a disrupting influence on the vortex. When the current is low and the vortex is weak, these droplets do not allow the vortex to form completely; so the resulting penetration is not as great as might have been expected. As the current becomes larger, the vortex becomes stronger and can impart angular momentum to the impacting droplets with less disruption. The resulting penetration is greater. Finally, when the current is large enough, the vortex is very strong and results in deep weld penetration.

2. Growth of the Finger Penetration.

As current is increased and overall weld penetration becomes larger, nearly all of the growth in penetration is a result of the growth in the finger penetration (see figure 18). Figure 20 shows that the finger penetration grows nearly as fast

as the total penetration. The result is a nearly constant depth for the "semicircular" region while the finger grows to over half of the total penetration. In many joint geometries this is not a desireable result. The narrow finger may not fill the bevel for instance, and cause incomplete fusion.

3. Distributed Source Conduction Solution.

The computer model used produces results that are of the right magnitude. But the predicted penetration grows too rapidly as current is increased. The assumptions of constant material properties and no convection as well as the use of a constant arc efficiency are responsible for the discrepancy.

4. Increased Penetration.

In order to realize increased penetration, a significantly larger amount of heat must be added to the plate. An attempt was made to use a high peak current balanced by a low base current so that the process would have the advantage of a current and yet still have a low average heat input. The attempt failed due to equipment deficiencies but the concept still has merit.

Another, possibly easier, way to acheive penetration through a tack weld without additional metal deposition would be the use of a second, non-consumable arc in the area of the tack weld. It is recommended for further study, that the use of a

second (possibly GTA) torch be tested on tack welded plates to determine the feasibility of its use and its most ideal location with relation to the GMA torch.

A. TEMPERATURE FIELD PROGRAM

1. Program Listing.

```
140 PRINT CHR$(147)

145 PRINT:PRINT:PRINT

150 PRINT"THIS COMPUTER PROGRAM WILL CALCULATE THE"

155 PRINT"TEMPERATURE FIELD PRODUCED BY A DISTRI-  "

160 PRINT"BUTED HEAT SOURCE TRAVELING ON A FINITE  "

165 PRINT"PLATE.  THE FORMULATION OF THIS SOLUTION"

170 PRINT"IS FROM A PAPER BY T.W. EAGAR AND        "

173 PRINT"N.-S. TSAI (WELDING JOURNAL, DEC, 1987   "

174 PRINT"RESEARCH SUPPLEMENT, PP 346S-355S.)      "

175 PRINT:PRINT:PRINT

180 PRINT"IT WILL STORE TEMPERATURE DATA IN YOUR   "

181 PRINT"DATA FILE.  WHAT IS THE NAME OF YOUR     "

183 INPUT"DATA FILE";B$

190 PRINT CHR$(147)

200 A=.147:RO=7.833:K1=.54

210 V=21:I=251:ETA=.75:V1=10

220 H=.9525:TN=20:SIGMA=.18897

270 OPEN 3,8,3,"@0:"+B$+",S,W"

280 DIM TT(60,20):DIM M(20)

300 INPUT"DO YOU WANT TO PRINT OUT THE TEMPERATURE DATA";PP$

310 IF PP$="N" THEN 490

410 OPEN 4,4

420 OPEN 2,4,2

430 OPEN 1,4,1
```

```
450 U$="99.9    9999   9999   9999   9999   9999   9999   9999"
455 U$=U$+"   9999   9999   9999"
460 PRINT#2,U$
490 GOTO 540
495 PRINT CHR$(147)
497 REM*************************BASE METAL PARAMETERS**********
500 INPUT"THERMAL DIFFUSIVITY (CM↑2/S)";A
510 INPUT"MASS DENSITY (G/CM↑3)";RO
520 INPUT"THERMAL CONDUCTIVITY (W/CM DEGREES C)";K1
540 PRINT"THERMAL DIFFUSIVITY =";A;"(W/CM DEGREES C)"
550 PRINT"MASS DENSITY =";RO;"(G/CM↑3)"
560 PRINT"THERMAL CONDUCTIVITY =";K1;"(W/CM DEGREES C)"
562 K=1E+7*K1:REM--THERMAL CONDUCTIVITY (G CM/S↑3 DEGREES C)
565 CP=K/(A*RO):REM--SPECIFIC HEAT (CM↑2/S↑2 DEGREES C)
570 INPUT"ARE THESE VALUES CORRECT";ZZ$
580 IF ZZ$="N" THEN 495
582 REM*****************************************************
583 REM
584 REM
585 REM
590 GOTO 650
595 PRINT CHR$(147)
597 REM*************************WELDING PARAMETERS************
600 INPUT"VOLTAGE (V)";V
605 INPUT"CURRENT (A)";I
610 INPUT"ARC EFFICIENCY";ETA
625 INPUT"TRAVEL SPEED (IN/MIN)";V1
```

```
635 INPUT"PLATE THICKNESS (2CM MAX)";H
638 INPUT"INITIAL TEMPERATURE (CELSIUS)";TN
645 INPUT"ARC DISTRIBUTION PARAMETER";SIGMA
650 PRINT"VOLTAGE =";V;"(V)"
655 PRINT"CURRENT =";I;"(A)"
660 PRINT"ARC EFFICIENCY =";ETA
665 PRINT"TRAVEL SPEED =";V1;"(IN/MIN)"
670 PRINT"PLATE THICKNESS =";H;"(CM)"
672 PRINT"INITIAL TEMPERATURE =";TN;"(DEGREES CELSIUS)"
674 PRINT"ARC DISTRIBUTION PARAMETER =";SIGMA
675 INPUT"ARE THESE VALUES CORRECT";ZZ$
680 IF ZZ$="N" THEN 595
681 Q=V*I*ETA:REM HEAT INPUT (J/S)
682 Q=1E+7*Q :REM HEAT INPUT(G CM↑2/S↑3)
683 VS=V1*2.54/60:REM TRAVEL SPEED(CM/S)
685 T=20:REM INTEGRATE OVER 20 SECONDS
696 REM********************************************************
697 REM
698 REM
699 PRINT CHR$(147)
700 INPUT"LONGITUDINAL OR TRANSVERSE (L OR T)";YY$
705 IF YY$="L" THEN 800
706 IF YY$="T" THEN 710
707 GOTO 700
708 REM********************************************************
710 PRINT "TRANSVERSE SECTION"
715 INPUT "X-DISTANCE IN CM OF SLICE FROM THE ARC (+ AHEAD,
```

```
    - BEHIND)";X
720 PRINT"X-DISTANCE =";X;"CM ":INPUT"IS THIS CORRECT (Y OR
    N)";ZZ$
725 IF ZZ$="N" THEN 710
730 ZT=INT(10*H):REM 1MM INCREMENTS
735 FOR ZS=0 TO ZT
740 Z=ZS*.1
745 FOR YS=0 TO 40
750 Y=YS*.1
760 GOTO850:REM****************TO SIMPSON'S INTEGRATION ROUTINE
765 TT(YS,ZS)=THETA+TN
770 NEXT YS
780 NEXT ZS
790 GOTO2000
793 REM*********************************************************
794 REM
795 REM
796 REM
799 REM********************************LONGITUDINAL SECTION****
800 PRINT "LONGITUDINAL SECTION"
805 INPUT "Y-DISTANCE (IN CM) OF SLICE FROM THE ARC
CENTERLINE";Y
810 PRINT"Y-DISTANCE =";Y;"CM ":INPUT"IS THIS CORRECT (Y OR
    N)";ZZ$
811 IF ZZ$="N" THEN 800
812 PRINT"AREA OF CALCULATION IS 6 CM LONG IN THE X-DIRECTION.
    INPUT FORWARDMOST"
```

```
813 INPUT"X COORDINATE (+ AHEAD OF ARC, - BEHIND)";X0

814 PRINT"X COORDINATE GOES FROM";X0;"CM TO "; X0-6;"CM

    (+ AHEAD OF ARC)"

815 INPUT"IS THIS CORRECT (Y OR N)";ZZ$

816 IF ZZ$="N" THEN 812

820 ZT=INT(10*H):REM 1MM INCREMENTS

825 FOR ZS=0 TO ZT

830 Z=ZS*.1

835 FOR XS=0 TO 60

840 X=X0-XS*.1

842 GOTO850:REM****************TO SIMPSON'S INTEGRATION ROUTINE

844 TT(XS,ZS)=THETA+TN

845 NEXT XS

846 NEXT ZS

847 GOTO 2100

848 REM********************************************************

849 REM

850 REM*************************BEGIN INTEGRATION SUBROUTINE***

870 DT=T/20 :REM*************DIVIDE TIME INTERVAL INTO 20 PARTS

880 REM ***SIMPSON'S RULE INTEGRAL*****************************

885 IN=0:N=0

887 N=N+1

890 FOR XX=0 TO18 STEP 2

900 T0=XX*DT

905 T1=(XX+1)*DT

908 IF T0<>0 THEN 910:REM ***********ZEROTH VALUE IS EQUAL TO 0

909 D0=0:GOTO 930
```

```
910 E0=((X↑2+Y↑2+2*X*VS*T0+VS↑2*T0↑2)/(4*A*T0+2*SIGMA↑2))+
    (Z↑2/(4*A*T0))

920 D0=EXP(-E0)*(T0↑-.5)/(2*A*T0+SIGMA↑2)

930 E1=((X↑2+Y↑2+2*X*VS*T1+VS↑2*T1↑2)/(4*A*T1+2*SIGMA↑2))+
    (Z↑2/(4*A*T1))

940 D1=EXP(-E1)*(T1↑-.5)/(2*A*T1+SIGMA↑2)

950 DI=D0*2+D1*4

980  IN=IN+DI

990 NEXT XX

1000  TO=DT*20:REM*********************LAST ELEMENT IN SIMPSON SUM

1005 E0=((X↑2+Y↑2+2*X*VS*T0+VS↑2*T0↑2)/(4*A*T0+2*SIGMA↑2))+
     (Z↑2/(4*A*T0))

1010 D0=EXP(-E0)*(T0↑-.5)/(2*A*T0+SIGMA↑2)

1020  IN=IN+D0

1023  IF N>1 THEN 1025

1024 Z=2*H-Z:GOTO887

1025  IF N>2 THEN 1030

1026 Z=2*H+Z:GOTO887

1030  IN=IN*DT/3

1050  THETA=IN*Q/PI*RO*CP*(4*PI*A)↑.5)

1055  IFYY$="L" THEN 844

1060  GOTO765:REM*******************************************************

1995  REM**************************************************PRINT OUT

2000  IF PP$="N"THEN2200

2001  PRINT#4,"TRANSVERSE SECTION AT X = ";X:PRINT#4:PRINT#4

2002  PRINT#4,"Y /Z     Z=0     Z=0.1  Z=0.2  Z=0.3  Z=0.4   ";

2003  PRINT#4,"Z=0.5  Z=0.6  Z=0.7  Z=0.8  Z=0.9":PRINT#4
```

```
2005 FOR YS=0 TO 40

2007 L=YS*.1

2010 FOR ZS=0 TO 9

2020 M(ZS)=TT(YS,ZS)

2030 PRINT#4,TT(YS,ZS)

2050 NEXT ZS

2060 PRINT#1,L;M(0);M(1);M(2);M(3);M(4);M(5);M(6);M(7);M(8);M(9)

2070 NEXT YS

2072 PRINT#4,"Y /Z     Z=0.1  Z=1.1  Z=1.2  Z=1.3  Z=1.4 ";

2073 PRINT#4 "Z=1.5  Z=1.6  Z=1.7  Z=1.8  Z=1.9":PRINT#4

2075 FOR YS=0 TO 40

2077 L=YS*.1

2080 FOR ZS=10 TO 19

2085 M(ZS)=TT(YS,ZS)

2092 NEXT ZS

2094 PRINT#1,L;M(10);M(11);M(12);M(13);M(14);M(15);M(16);M(17);
     M(18);M(19)

2096 NEXT YS

2098 GOTO2200:REM**********************************************

2100 IFPP$="N"THEN2200

2101 PRINT"4,"LONGITUDINAL SECTION AT Y = ";Y:PRINT"4:PRINT#4

2102 PRINT#4,"Y /Z     Z=0     Z=0.1  Z=0.2  Z=0.3  Z=0.4  ";

2103 PRINT#4,"Z=0.5  Z=0.6  Z=0.7  Z=0.8  Z=0.9":PRINT#4

2105 FOR XS=0 TO 60

2107 L=X0-XS*.1

2110 FOR ZS=0 TO 9

2120 M(ZS)=TT(XS,ZS)
```

```
2130 PRINT#3,TT(XS,ZS)

2150 NEXT ZS

2160 PRINT#1,L;M(0);M(1);M(2);M(3);M(4);M(5);M(6);M(7);M(8);M(9)

2170 NEXT XS

2172 PRINT#4,"Y /Z    Z=1.0  Z=1.1  Z=1.2  Z=1.3  Z=1.4  ";

2173 PRINT#4,"Z=1.5  Z=1.6  Z=1.7  Z=1.8  Z=1.9":PRINT#4

2175 FOR XS=0 TO 60

2177 L=X0-XS*.1

2180 FOR ZS=10 TO 19

2185 M(ZS)=TT(XS,ZS)

2192 NEXT ZS

2194 PRINT#1,L;M(10);M(11);M(12);M(13);M(14);M(15);M(16);M(17);

     M(18);M(19)

2198 NEXT XS

2200 FORZS=0TOZT

2210 IF YY$="L"THEN2220

2215 QQ=40:GOTO2230

2220 QQ=60

2240 FOR XS=0TOQQ

2260 PRINT#3,TT(XS,ZS)

2270 NEXT XS

2280 NEXT ZS

2290 CLOSE 1:CLOSE 2:CLOSE 3:CLOSE 4
```

2. Program Explanation.

Lines 140-175:

Clear the screen and prints a message.

Lines 180-183:

Prompt the user for the name of his data file and puts it into the string variable, B$.

Lines 190-220:

Clear the screen and assign initial values to the thermal diffusivity (A), mass density (RO), thermal conductivity (K1), voltage (V), current (I), arc efficiency (ETA), arc travel speed (V1), plate thickness (H), initial temperature (TN) and arc distribution parameter (SIGMA).

Line 270:

Opens the data file.

Line 280:

Dimensions the temperature arrays.

Lines 300-460:

Ask the user if he wants the data printed on the printer in addition to recording it in his data file. If the answer is anything but "N", it opens the print files. The first file (#4) is the verbatim file. Anything printed in file #4 will be printed verbatim. The second file (#2) is the format file. The characters printed in file #2, in lines 450-460,

format the Commodore 802 printer so that anything printed in the third file (#1) will be printed in that format.

Lines 490-580:

Initially skip the input and print the current values of the Base Metal Parameters. Line 570 asks if these values are correct. If not, line 580 branches back to allow the input of new values.

Lines 582-585:

Remarks.

Lines 590-680:

Perform the same function as lines 490-580 for the Welding Parameters.

Lines 681-699:

Calculate the heat per unit time actually applied to the plate. The arc efficiency was obtained from reference [6] page 164. Line 682 converts Q to the right units and line 683 converts the travel speed from ipm to cm/s. Line 685 sets the time over which the integration will take place.

Lines 700-709:

Allow the user to select a longitudinal cut parallel to the direction of travel or a transverse cut perpendicular to it.

Lines 710-796:

Set up the location identification for the transverse cut. Lines 715-725 allow the user to input the x

location of the transverse cut. Line 730 sets ZT equal to the thickness of the plate in integer millimeters. Line 735 is the beginning of the loop for the z dimension (measured down from the surface of the plate) and line 740 causes Z to be in centimeters. Line 745 is the beginning of the loop for the y dimension (0 to 40mm) off thte centerline of the weld. Line 750 causes Y to be in centimeters. Line 760 branches to the Simpson's Rule Integration routine. The result is THETA = T - TN, so the initial temperature is added in line 765 to get the temperature at that location. Lines 770 and 780 are the ends of the nested loops and line 790 branches to the output.

Lines 799-849:

Set up the location identification for the longitudinal cut. Lines 805-811 allow the user to input the distance of the longitudinal cut from the centerline of the weld. Lines 812-816 allow the user to select the location of the 6cm (along the length of the weld) on which temperature calculations are to be conducted. Line 820 sets ZT equal to the plate thickness in integer millimeters. Line 825 is the beginning of the loop for the z dimension (measured down from the surface of the plate) and line 830 converts z into centimeters. Line 835 is the beginning of the loop for the x dimension (measured

from the x location input in line 813). Line 840 converts x into centimeters and starts the measurement at the x value input in line 813. Line 842 branches to the Simpson's Rule Integration routine. The result is THETA = T - TN so the initial temperature is added in line 844 to get the temperature at that location. Lines 845 and 846 are the ends of the nested loops and line 847 branches to the output.

Lines 850-1060:

Are the Simpson's Rule Integration routine. Lines 850-890 divide the time interval into twenty parts, set the sum (IN) and the counter (N) to their initial values and start the loop. Lines 900 and 905 identify the ends of the incremental time element. Lines 908-909 handle the case when T0 equals 0 and avoids division by zero. Lines 910-940 calculate the partial sums of the integral using the equation from chapter 6. Lines 950-980 apply the Simpson's multipliers and increase the value of the sum (IN). Line 990 is the end of the integral loop. Lines 1000-1020 calculate and add the last term in the Simpson's Rule expansion. Lines 1023-1026 add the virtual heat sources at H below the plate and 2H above the plate (where H is the plate thickness) and superpose the solutions. Line 1030 completes the Simpson Integration. Line 1050 multiplies the result by the constants in front of the integral sign (see the equation in chapter 6). Lines

1055 and 1060 return to where the subroutine was called. NOTE: Originally GOSUB/RETURN statements were used but these take more computer time so GOTO statements were used instead.

Lines 1935-2290:

Are the output section. Since much of the output programming is computer specific and in general for cosmetic purposes only, it will not be discussed in depth. It suffices to say that the program prints out the temperature data if that was desired and records the same data in the user's data file. The last line closes all the files to avoid data loss.

B. COMPUTER PROGRAM OUTPUT

```
WELD 1-1:   I=251A, V=21V, Arc Eff.=0.75, TS=10ipm, Plt Thk=.95cm
            Initial Temp.=20 deg.C, Arc Dist. Parameter=0.18897
 (cm)       Y = 0cm (Weld Centerline)     Max. Penetration =0.13cm
 Z =   0.0   0.1   0.2   0.3   0.4   0.5   0.6   0.7   0.8   0.9
 X =  ----- ----- ----- ----- ----- ----- ----- ----- ----- -----
 1.0    110   110   109   106   102    97    93    89    87    85
  .9    146   146   144   139   133   126   120   114   110   108
  .8    194   194   190   183   174   164   155   146   140   137
  .7    257   256   250   240   227   213   199   187   179   174
  .6    335   334   325   311   294   274   255   238   226   220
  .5    430   428   417   398   374   347   322   300   283   275
  .4    542   540   525   500   468   434   400   371   350   339
  .3    669   666   647   616   576   532   489   453   426   412
  .2    808   804   781   742   693   639   587   542   509   493
  .1    953   948   920   874   815   752   689   636   597   577
 0.0   1097  1091  1059  1006   938   865   793   732   687   663
- .1   1233  1226  1191  1131  1055   973   893   824   774   747
- .2   1352  1345  1307  1242  1160  1070   983   908   854   826
- .3   1448  1441  1401  1333  1247  1152  1060   982   924   894
- .4   1515  1509  1468  1393  1311  1214  1121  1040   981   951
- .5   1550  1545  1505  1438  1350  1255  1162  1082  1024   994
- .6   1554  1550  1513  1448  1364  1273  1183  1106  1051  1022
- .7   1527  1525  1492  1432  1355  1269  1186  1115  1063  1036
- .8   1476  1477  1448  1395  1325  1248  1173  1108  1062  1038
- .9   1407  1409  1386  1340  1280  1213  1147  1091  1050  1030
-1.0   1326  1330  1312  1275  1225  1168  1113  1065  1031  1014
-1.1   1239  1246  1234  1205  1164  1118  1073  1034  1006   993
-1.2   1153  1163  1155  1134  1103  1067  1032  1001   980   970
-1.3   1073  1084  1081  1067  1045  1018   991   969   953   946
-1.4   1000  1012  1014  1006   991   972   954   937   926   922
-1.5    936   950   955   952   943   932   919   909   902   900
-1.6    881   896   904   905   902   896   889   883   879   879
-1.7    836   851   861   866   866   864   862   859   858   860
-1.8    797   813   825   832   836   837   837   838   839   842
-1.9    765   782   794   803   809   813   816   818   821   825
-2.0    737   754   767   778   785   791   796   800   804   809
-2.1    713   730   744   755   764   771   777   782   787   793
-2.2    692   709   723   735   744   752   759   766   771   777
-2.3    672   689   703   715   726   735   742   749   755   761
-2.4    654   671   685   697   708   718   726   733   740   746
-2.5    637   653   668   680   691   701   710   717   724   731
-2.6    621   637   651   664   675   685   694   702   709   715
-2.7    606   621   636   648   660   670   679   687   694   701
-2.8    591   607   621   633   645   655   664   672   680   686
-2.9    577   593   606   619   630   641   650   658   666   672
-3.0    564   579   593   605   617   627   636   644   652   659
-3.1    552   566   580   592   603   614   623   631   639   646
-3.2    540   554   567   580   591   601   610   619   626   633
-3.3    528   542   556   568   579   589   598   606   614   621
-3.4    518   531   544   556   567   577   586   595   602   609
-3.5    507   521   533   545   556   566   575   583   591   598
```

TRANSVERSE SECTION

WELD 1-1: I=251A, V=21V, Arc Eff.=0.75, TS=10ipm, Plt Thk=.95cm
Initial Temp.=20 deg.C, Arc Dist. Parameter=0.18897
Transverse Cut at X = -0.6 Max. Penetration=0.13cm

(cm) Z = Y =	0.0	0.1	0.2	0.3	0.4	0.5	0.6	0.7	0.8	0.9
0.0	1554	1550	1513	1448	1364	1273	1183	1106	1051	1022
.1	1536	1532	1496	1432	1350	1259	1171	1096	1041	1013
.2	1484	1481	1446	1385	1307	1221	1137	1064	1012	985
.3	1402	1400	1368	1312	1239	1159	1082	1015	966	941
.4	1296	1295	1267	1217	1152	1080	1010	950	907	884
.5	1174	1174	1150	1107	1051	988	927	875	837	818
.6	1044	1044	1025	989	941	889	837	793	761	745
.7	912	913	898	869	831	783	746	710	683	670
.8	785	787	776	753	723	689	656	627	607	597
.9	667	670	662	646	623	597	572	550	534	526
1.0	562	565	561	549	532	513	494	478	467	461
1.1	470	474	472	464	452	439	425	414	406	402
1.2	392	396	396	391	383	374	365	357	352	350
1.3	327	331	332	329	325	319	313	308	305	304
1.4	274	278	279	278	276	272	269	266	264	263
1.5	230	234	236	236	235	233	231	230	229	229
1.6	195	199	200	201	201	200	200	199	199	199
1.7	166	169	171	172	173	173	173	173	173	173
1.8	142	145	147	148	149	150	150	150	151	151
1.9	123	125	127	128	129	130	131	131	132	132
2.0	107	109	110	112	113	114	114	115	115	116
2.1	93	95	96	98	99	100	100	101	101	102
2.2	82	83	85	86	87	88	88	89	89	90
2.3	72	74	75	76	77	77	78	79	79	80
2.4	64	65	66	67	68	69	69	70	70	71
2.5	57	58	59	60	61	61	62	62	63	63
2.6	52	53	53	54	55	55	56	56	56	57
2.7	47	48	48	49	49	50	50	51	51	51
2.8	43	43	44	44	45	45	46	46	46	47
2.9	39	40	40	41	41	41	42	42	42	42
3.0	36	37	37	37	38	38	38	39	39	39
3.1	34	34	34	35	35	35	36	36	36	36
3.2	32	32	32	32	33	33	33	33	34	34
3.3	30	30	30	31	31	31	31	31	31	32
3.4	28	28	29	29	29	29	29	30	30	30
3.5	27	27	27	27	28	28	28	28	28	28
3.6	26	26	26	26	26	27	27	27	27	27
3.7	25	25	25	25	25	25	26	26	26	26
3.8	24	24	24	24	25	25	25	25	25	25
3.9	23	23	24	24	24	24	24	24	24	24
4.0	23	23	23	23	23	23	23	23	23	23

Material Parameters Used: Thermal Diffusivity = 0.147 [cm↑2/s]
Mass Density = 7.833 [g/cm↑3]
Thermal Conductivity=0.54[W/cm-deg.C]

REFERENCES

[1] Lin, M.L. and T.W. Eager, "Influence of Arc Pressure on Weld Pool Geometry," THE WELDING JOURNAL, v.64 (6), June 1985, Research Supplement, pp 163-s to 169-s.

[2] American Welding Society, CURRENT WELDING PROCESSES, AWS, New York, New York, 1964, pp 23, 66.

[3] Masubuchi, K., "Metal Transfer in Welding Arcs and Melting of Electrodes," Classnotes for Welding Engineering, MIT, Cambridge, MA, pp 3-1 to 3-57.

[4] Lesnewich, A., "Control of Melting Rate and Metal Transfer in Gas-Shielded Metal-Arc Welding Part 1--Control of Electrode Melting Rate," THE WELDING JOURNAL, v.37 (8), 1958, Research Supplement, pp 343-s to 353-s.

[5] Sanders, N.A. and E. Pfender, "Measurement of Anode Falls and Anode Heat Transfer in Atmospheric Pressure High Intensity Arcs," JOURNAL OF APPLIED PHYSICS, v.55 (3), February 1984, pp 714-722.

[6] International Institute of Welding, THE PHYSICS OF WELDING, 2nd edition, J.F. Lancaster [ed.], Pergamon Press, Oxford/New York, 1986, pp 9-46, 146-299.

[7] Lesnewich, A., "Control of Melting Rate and Metal Transfer in Gas-Shielded Metal-Arc Welding Part 11--Control of Metal Transfer," THE WELDING JOURNAL, v.37 (9), 1958, Research Supplement, pp 418-s to 425-s.

[8] Jackson, C.E., "The Science of Arc Welding," THE WELDING JOURNAL, v.39 (4,5,6), 1960, Research Supplement, pp 129-s to 140-s, 177-s to 189-s, 225-s to 230-s.

[9] Quigley,M.B.C., P.H. Richards, D.T. Swift-hook and A.E.F. Gick, "Heat Folw to the Workpiece from a TIG Welding Arc," JOURNAL OF PHYSICS D: APPLIED PHYSICS, v.6, 1973, pp 2250-2256.

[10] Dinulescu, H.A. and E. Pfender, "Analysis of the Anode Boundary Layer of High Intensity Arcs," JOURNAL OF APPLIED PHYSICS, v.51 (6), 1980, p. 3154.

[11] Christensen, N., V. Davies and K. Gjermundsen, "Distribution of Temperatures in Arc Welding," BRITISH WELDING JOURNAL, v.12 (2), February 1985, pp 54-75.

[12] Amin, M. and Naseer Ahmed, "Synergic Control in MIG Welding," THE RESEARCH BULLETIN, v.27 (5), May 1986, pp 149-205.

[13] Yeo, Ralph, "Put Your Finger on the Pulse of MIG Welding at WELDEX," METAL CONSTRUCTION, v.15 (9), September 1983, pp 20-25.

[14] Eager, T.W. and N.-S. Tsai, "Temperature Fields Produced by Traveling Distributed Heat Sources," THE WELDING JOURNAL, v.62 (12), December 1983, Research Supplement, pp 346-s to 355-s.

[15] Essers, W.G. and R. Walter, "Heat Transfer and Penetration Mechanisms with GMA and Plasma-GMA Welding," THE WELDING JOURNAL, v.60 (2), February 1981, Research Supplement, pp 37-s to 42-s.

[16] Mills, G.S., "Fundamental Mechanisms of Penetration in GTA Welding," THE WELDING JOURNAL, v.58 (1), January 1979, Research Supplement, pp 21-s to 24-s.

[17] Ishizaki, K. "A New Approach to the Mechanism of Penetration," THE WELDING INSTITUTE INTERNATIONAL CONFERENCE, London, April 15-17, 1980, pp 65-76.

[18] Oreper, G.M., T.W. Eagar and J. Szekely, "Convection in Arc Weld Pools," THE WELDING JOURNAL, v.62 (11), November 1983, Research Supplement, pp 307-s to 312-s.

[19] Agapakis, J., "Closed-Loop Welding Analysis Study, Appendix B - Weld Bead Geometry Prediction: A Review of the Current State of the Art," MIT Technical Report No. 92830 submitted to: Department of the Navy, Naval Ocean Systems Center, September 1983, pp B1-B7.

[20] Masubuchi, K., ANALYSIS OF WELDED STRUCTURES, Pergamon Press, Oxford/New York, 1980, pp 60-75.

[21] Lancaster, J.F., METALLURGY OF WELDING, 3rd edition, George Allen & Unwin Publishers, London, 1980, pp 17-50.

[22] American Welding Society, WELDING HANDBOOK, 7th edition, vols. I & II, AWS, Miami, FL, 1976.

[23] Shraerman, M.R., "Nomograms for Determining the Main Parameters of Multipass Welding," WELDING PRODUCTION, v.29 (11), November 1982, pp 10-12.

[24] Salter, G.R. and J. Doherty, "Procedure Selection for Arc Welding," METAL CONSTRUCTION, V.13 (9), September 1981, pp 20-26.

[25] Chihoski, R., "The Rationing of Power Between the GTA and Electrode," WELDING JOURNAL, v.49 (2), February 1970, Research Supplement, pp 69-s to 82-s.

[26] Kolodziejczak, G.C., "GMAW Control to Minimize Interference From Tack Weld," Ph.D. thesis, Massachusetts Institute of Technology, June 1987.

[27] Rosenthal, D., "The Theory of Moving Source of Heat and Its Application to Metal Treatment," TRANSACTIONS ASME, v.43 (11), November 1946, pp 849-866.

21 847

Thesis
S66778 Spencer
c.1 Penetration effects of
the compound vortex in
gas metal-arc welding.

Thesis
S66778 Spencer
c.1 Penetration effects of
the compound vortex in
gas metal-arc welding.

AMERICAN BINDERY
TOPEKA KANSAS

thesS66778
Penetration effects of the compound vort
3 2768 000 79177 6
DUDLEY KNOX LIBRARY